RESEARCH ARTICLE

Retinal Remodeling in the Tg P347L Rabbit, a Large-Eye Model of Retinal Degeneration

Bryan William Jones,[1*] Mineo Kondo,[2] Hiroko Terasaki,[2] Carl Brock Watt,[1] Kevin Rapp,[1] James Anderson,[1] Yanhua Lin,[1] Marguerite Victoria Shaw,[1] Jia-Hui Yang,[1] and Robert Edward Marc[1]

[Jia-Hui should be hyphenated]

[1]Department of Ophthalmology, Moran Eye Center, University of Utah, Salt Lake City, Utah 84132

AQ1   [2]Department of Ophthalmology, Graduate School of Medicine, Nagoya University, Nagoya, Japan   *466-8560*

ABSTRACT

Retinitis pigmentosa (RP) is an inherited blinding disease characterized by progressive loss of retinal photoreceptors. There are numerous rodent models of retinal degeneration, but most are poor platforms for interventions that will translate into clinical practice. The rabbit possesses a number of desirable qualities for a model of retinal disease including a large eye and an existing and substantial knowledge base in retinal circuitry, anatomy, and ophthalmology. We have analyzed degeneration, remodeling, and reprogramming in a rabbit model of retinal degeneration, expressing a rhodopsin proline 347 to leucine transgene in a TgP347L rabbit as a powerful model to study the pathophysiology and treatment of retinal degeneration. We show that disease progression in the TgP347L rabbit closely tracks human cone-sparing RP, including the cone-associated preservation of bipolar cell signaling and triggering of reprogramming. The relatively fast disease progression makes the TgP347L rabbit an excellent model for gene therapy, cell biological intervention, progenitor cell transplantation, surgical interventions, and bionic prosthetic studies. J. Comp. Neurol. 000:000–000, 2011.

© 2011 Wiley-Liss, Inc.

INDEXING TERMS: retinitis pigmentosa; retinal degeneration; retinal remodeling; neural remodeling; transgenic; electron microscopy; light microscopy; confocal microscopy; electroretinogram; computational molecular phenotyping; human; rabbit

Although a number of animal models of retinal degeneration have been discovered or produced (Petersen-Jones, 1998; Chader, 2002; Baehr and Frederick, 2009) exhibiting varying rates of progression or features of retinal degeneration including remodeling (Jones et al., 2003; Marc and Jones, 2003; Marc et al., 2003), practical large animal models of retinitis pigmentosa (RP) are rare. However, they are desirable for surgical interventions, subretinal injections of gene therapies (Acland et al., 2001; Bainbridge et al., 2008; Maguire et al., 2008), survival factors (Faktorovich et al., 1990, 1992; Zeiss et al., 2006; Beltran et al., 2007), cells or cellular components (Young et al., 2000; Gias et al., 2007; Vugler et al., 2007), and bionic interventions (Humayun et al., 1996; Lakhanpal et al., 2003; Eckhorn et al., 2006; Yanai et al., 2007).

The development of the TgP347L rabbit model of autosomal dominant RP (adRP) (Kondo et al., 2009), allowed us to compare disease sequelae and features with human RP. In short, we found that the TgP347L rabbit mimics the autosomal dominant focal, cone-sparing RP found in human (Marc et al., 2007), and TgP347S porcine models (Petters et al., 1997). Rabbit TgP347L rod photoreceptors survive for up to 12–16 weeks, and cone photoreceptors survive for up to 40 weeks; however, during this time, rod bipolar cells switch their phenotype by expressing ionotropic glutamate receptors (iGluRs). It is also hypothesized that the rod bipolar cells effectively lose rod contacts and make ectopic cone contacts, expressing iGluRs. By 40 weeks, some opsin expression can be found in cones, albeit delocalized. However, the presence of cones appears to prevent gross topographic retinal restructuring, although early sprouting events are

occurring including extreme retinal remodeling of horizontal cells and bipolar cells. Disease progression in the TgP347L rabbit model appears to closely resemble that of human cone-sparing RP, and will facilitate the continued exploration of axonogenesis, neuritogenesis, and retinal remodeling in RP and allied diseases. Additionally, the large eye allows for a more convenient model for cell transplantation, surgical interventions, and exploration of bionic prosthetic studies.

MATERIALS AND METHODS

Rabbits

Adult male TgP347L rabbits (aged 12, 16, and 40 weeks) were generated in the Kondo laboratory in Nagoya, Japan. Our technique for generation of Tg rabbits has been described in detail (Kondo et al., 2009). Briefly, a rabbit rhodopsin BAC clone that included the entire rhodopsin gene was identified, and a C-to-T transition at the codon of proline 347 was performed by BAC recombination. This transition in exon 5 of the rabbit rhodopsin gene resulted in a proline-to-leucine substitution at codon 347. Following the BAC modification in *E. coli*, the linearized BAC Tg construct was purified and injected into rabbit embryos at the pronucleus stage. Southern blots showed that 12 of 80 newborn rabbits were transgene positive, and 10 of the 12 survived. These initial 10 transgenic founders were backcrossed to New Zealand White wild-type rabbits for three generations, and six founders were found to transmit the transgene. Wild-type rabbits were derived form littermates of the founder rabbits. We mainly reproduced and investigated line 7, which had the highest level of transgene expression and the most severe photoreceptor degeneration as determined histologically. The ratio of transgene to endogeneous opsin mRNA was 4:1 in line 7 (Kondo et al., 2009). Prior to tissue harvest, TgP347L rabbits were euthanized via intraperitoneal urethane, and the eyes were enucleated. All animal experiments were conducted according to the ARVO Statement for the Use of Animals in Ophthalmic and Vision Research, with approval of the Institutional Animal Care Committee at the University of Utah.

Human tissue

Human RP tissue was obtained from The Foundation Fighting Blindness Retina Donor Program and the University of Utah Lions Eye Bank. Institutional approval for use of human eyes was obtained from the University of Utah and followed the tenets of the Declaration of Helsinki. All retinal tissues and data were de-identified in accordance with HIPPA Privacy Rules.

Electroretinography (ERG)

ERG was performed to assess the state of rod loss prior to tissue harvest. Rabbits were dark-adapted for 60 minutes, and then anesthetized with an intramuscular injection of 25 mg/kg ketamine and 2 mg/kg xylazine. ERGs were recorded with a Ganzfeld bowl and Burian-Allen bipolar contact lens electrodes (Hansen Laboratory, Iowa, City, IA). Eight steps of stimulus intensities ranging from -4.8 to 2.2 log cd s m^{-2} were used for the scotopic ERG recordings, and four steps of stimuli ranging from -0.8 to 2.2 log cd s m^{-22} for the photopic ERGs. The photopic ERGs were recorded on a rod-suppressing white background of 1.3 log cd m^{-2}. Signals were amplified, bandpass-filtered between 0.3 and 1,000 Hz, and averaged by using a computer-assisted signal analysis system (MEB-9100, Neuropack, Nihon Kohden, Tokyo, Japan).

Cryosection immunocytochemistry

Eyecups were processed immediately into 4% paraformaldehyde overnight. Samples were removed from sclera, cryoprotected in sucrose buffer at 10%, 20%, and 30%, and then sectioned for confocal microscopy at 20 µm on a cryostat. Slides were stored at $-20°$C until used. When used, slides were warmed at 37°C for 30 minutes and soaked in phosphate buffer for 30 minutes prior to antibody exposure. Antibodies and their specificities are given in Tables 1 and 2. Primary antibodies were incubated overnight at 4°C. For metabotropic glutamate receptor 6 (mGluR6), cellular retinaldehyde binding protein (CRALBP), cone arrestin, LWS opsin, and protein kinase C α (PKCα), signals were visualized with Cy3. For calbindin, rhodopsin 1D4, and glutamine synthetase (GS), incubation was performed overnight at 4°C and visualized with Alexa Fluor 647. DAPI was used as a nuclear stain at 10 µm for 10 minutes with a 10-minute rinse. Secondary antibodies were indocarbocyanine (Cy3) goat anti-rabbit, and Alexa Fluor 594 goat anti-rabbit and Alexa Fluor 647 goat anti-mouse. No labeling was seen when Cy3-conjugated IgG or Alexa Fluor 594/647-conjugated IgG was applied without primary antibodies.

Abbreviations	
AGB	1-Amino-4-guanidobutane
BSA	Bovine serum albumin
CRALBP	Cellular retinaldehyde binding protein
GABA	γ-Aminobutyric acid
GCL	Granular cell layer
GS	Glutamine synthetase
iGluR	Ionotropic glutamate receptor
INL	Inner cell layer
IPL	Inner plexiform layer
KA	Kainate
mGluR	Metabotropic glutamate receptor
ONL	Outer cell layer
OPL	Outer plexiform layer
PKC	Protein kinase C
RPE	Retinal pigment epithelium

2   The Journal of Comparative Neurology | Research in Systems Neuroscience

ID: **jaishankarn** | Black Lining: **[ON]** | Time: **18:01** | Path: **N:/3b2/CNE#/Vol51913/110135/APPFile/JW-CNE#110135**

TABLE 1.

Primary Antibodies Used in This Study

Antibody	Immunogen, Host Species	Source	Dilution used
AGB	BSA-glutaraldehyde- (1-amino-4-guanidobutane) conjugate, rabbit	Signature Immunologics B100/rabbit-polyclonal	1:4.000
L-aspartate	BSA-glutaraldehyde- (L-aspartate) conjugate, rabbit	Signature Immunologics D100/rabbit-polyclonal	1:2.000
L-glutamate	BSA-glutaraldehyde- (L-glutamate), conjugate, rabbit	Signature Immunologics E100/rabbit-polyclonal	1:32.000
Glycine	BSA-glutaraldehyde- (glycine) conjugate, rabbit	Signature Immunologics G100/rabbit-polyclonal	1:4.000
Glutathione	BSA-glutaraldehyde- (glutathione) conjugate, rabbit	Signature Immunologics J100/rabbit-polyclonal	1:4.000
L-glutamine	BSA-glutaraldehyde- (L-glutamine) conjugate, rabbit	Signature Immunologics Q100/rabbit-polyclonal	1:4.000
Taurine	BSA-glutaraldehyde- (taurine) conjugate, rabbit	Signature Immunologics TT100/rabbit-polyclonal	1:16.000
GABA	BSA-glutaraldehyde- (4-aminobutyrate) conjugate, rabbit	Signature Immunologics YY100/rabbit-polyclonal	1:32.000
Rod opsin 1D4	C-terminal peptide TETSQVAPA-COOH, mouse	R. Molday, University of British Columbia-monoclonal	1:4.000
mGluR6	C-terminal peptide KKTSTMAAPPQNENAEDAK of the mGluR6 sequence, rabbit	S.C. Massey, University of Texas Graduate School of Biomedical Sciences-polyclonal	1:1.000
CRALBP	Cellular retinaldehyde-binding protein isolated from retina and RPE, rabbit	J.C. Saari, University of Washington-polyclonal	1:1.000
PKCα	Synthetic peptide corresponding to amino acids 659–672 from the C-terminal variable (V5) region of rat PKCα, mouse	Sigma (#P-4334)-polyclonal	1:1.000
Cone arrestin	Synthetic peptide from the C-terminal EVATEVPFRLMHPQPED corresponding to amino acids 2–18 of rat visual arrestin, rabbit	Calbiochem #178605-polyclonal	1:1.000
Calbindin	Calbindin-D 28 kDa from chicken gut, mouse	Sigma #C-8666-monoclonal	1:1.000
Red/green opsin	Recombinant human red/green opsin targeting the last 38 amino acids from the C-terminus, rabbit	Chemicon #AB5405 now Millipore # AB5405-polyclonal	1:1.000
Glutamine synthetase	Generated from glutamine synthetase corresponding to amino acids 1–373 from the C-terminal region, mouse.	Transduction Labs #G-45020-monoclonal	1:1.000

For abbreviations, see list.

Computational molecular phenotyping (CMP)

Retinal neurons were classified by CMP per (Marc and Jones, 2002) by using an array of small-molecule signatures (L-aspartate, L-glutamate, glycine, L-glutamine, glutathione, γ-aminobutyric acid [GABA], taurine) in addition to antibodies targeting rod opsin, LWS opsin, and CRALBP. Briefly, isolated eyes were hemisected and immersion-fixed overnight in 1% paraformaldehyde, 2.5% glutaraldehyde, 3% sucrose, 0.01% $CaCl_2$, in 0.1 M phosphate buffer, pH 7.4. Tissues were then dehydrated in graded methanols and acetone and embedded in epoxy resin. Tissues were then serial sectioned at 200 nm onto 12-spot Teflon-coated slides (Cel-Line, Fisher Scientific, Waltham, MA). Antibody exposure and silver intensification is described below under antibody characterization. Cell classification was performed on N-dimensional monochrome images by K-means clustering (Marc et al., 1995; Marc and Cameron, 2002; Marc and Jones, 2002) using pixel-based approaches, and data clusters were visualized as theme maps (PCI Geomatica from PCI Geomatics, Richmond Hill, ON, Canada and CMP, a clustering package created at the Scientific Computing Institute, University of Utah, Salt Lake City, UT). Adobe Photoshop CS5 (Adobe Systems, San Jose, CA) was used for final image generation. Incubation of all antibodies gener-

TABLE 2.

IgG Competitive Sensitivities Computed From Inhibition Assays[1]

Bis-conjugate	D	E	G	J	Q	τ	γ
D	0	5	10	9	7	6	6
E	7	0	9	9	5	6	4
G	8	5	0	9	7	6	6
J	9	4	9	0	6	5	5
Q	9	5	9	9	0	6	6
τ	8	5	10	9	7	0	5
γ	10	5	8	9	7	6	0

[1]Expressed as log differential inhibition: log [C]/[T], where [C] and [T] are the concentrations of any conjugate (C) or the cognate target conjugate (T) required for 100% binding block. D, aspartate; E, glutamate; G, glycine; J, glutathione; Q, glutamine; τ, taurine; γ, γ-aminobutyric acid (GABA).

ated against small-molecular targets and rhodopsin 1D4 was performed overnight at room temperature, and visualization was with goat anti-rabbit secondary IgG coated with 1-nm gold (Amersham, Arlington Heights, IL) and silver-intensified (Kalloniatis and Fletcher, 1993).

AGB preparation

Some retinas were removed and hemisected with large retinal pieces mounted on cellulose acetate filter discs

and incubated in vitro for excitation mapping with 1-amino-4-guanidobutane (AGB). AGB is an organic cation that permeates activated α-amino-3-hydroxyl-5-methylisoxazole-4-propionic acid (AMPA), kainate (KA), and N-methyl-D-aspartate (NMDA) iGluR gated channels (Marc, 1999c) as well as mGluR6 receptor-mediated channels on ON bipolar cells (Kalloniatis et al., 2004; Marc et al., 2005b). Retinas were incubated for 10 minutes at 35°C in oxygenated Ames-HEPES medium + 5 mM AGB with and without iGluR agonists (KA 25 μm, NMDA 1 mM), followed by fixation in conventional aldehydes (see below).

Small-molecular antibody characterization

Anti-hapten IgGs from Signature Immunologics (Salt Lake City, UT; Table 1) have been extensively characterized in prior publications (Marc et al., 1995; Marc, 1999a,b; Marc and Cameron, 2002; Marc and Jones, 2002). Each is an IgG isotype (determined by affinity chromatography and immunoblotting) produced in rabbit hosts immunized with glutaraldehyde-amino acid conjugates to bovine serum albumin (BSA) as described in Marc et al. (1995). Four analysis types were used to characterize the specificity and detectivity of each anti-hapten IgG: 1) dependence on target molecule trapping; 2) immunodot assays against cognate small molecule–protein conjugates; 3) competition assays against free and bisconjugates of small molecules (Table 2); 4) binding curves on quantitative artificial antigen stacks; and 5) cluster analysis (Marc et al., 1995).

The AGB antibody recognizes an AGB–glutaraldehyde conjugate and was designed to detect exogenously applied AGB as a tracer molecule of glutamate-mediated ionotropic activity (Marc, 1999a,b; Marc et al., 2005b). Results corresponded to previous results in normal and degenerate mouse and human retina (Marc et al., 2007).

The antibody against L-aspartate has been used to detect the presence and concentration of aspartate in retinal tissues (Marc et al., 1995, 1998a,b; Kalloniatis et al., 1996; Marc and Jones, 2002). Differential labeling of aspartate in retina reveals its presence in rods and retinal neurons at low levels, but also in isolated cells at higher concentrations that appear to be undergoing apoptosis, particularly in the photoreceptor cell layer. Results corresponded to previous results in normal and degenerate mouse and human retina (Marc et al., 2007).

The antibody against L-glutamate used to examine the presence and concentration of glutamate labeling in retina follows that previously described (Davanger et al., 1991; Grunert and Martin, 1991; Crooks and Kolb, 1992; Martin and Grunert, 1992; Kalloniatis et al., 1996). Results corresponded to previous results in normal and degenerate mouse and human retina (Marc et al., 2007).

The glycine antibody was used to examine the presence and concentration of glycine, which always co-localizes with significant glutamate signals in most presumed glycinergic amacrine cells and in ON cone bipolar cells (Marc et al., 1995, 1998b; Kalloniatis et al., 1996; Marc and Jones, 2002). Results corresponded to previous results in normal and degenerate mouse and human retina (Marc et al., 2007).

The glutathione antibody has been used to identify the presence and concentration of glutathione in Müller glia and horizontal cells (Marc et al., 1995, 1998a,b; Pow and Crook, 1995; Kalloniatis et al., 1996; Marc and Jones, 2002). Results corresponded to previous results in normal and degenerate retina (Marc et al., 2007) indicating early remodeling of horizontal cell processes, photoreceptor stress, and metabolic alterations in Müller glia (Marc et al., 2008).

The L-glutamine antibody was used to detect L-glutamine that is present in most retinal neurons, but particularly retinal Müller cells. Glutamine is also present at high levels in the retinal pigment epithelium (RPE). Results corresponded to previous results in normal and degenerate retina (Marc et al., 2007) indicating early remodeling of horizontal cell processes, photoreceptor stress, and metabolic alterations in Müller glia (Marc et al., 2008).

The taurine antibody was used to detect free taurine concentrations in most retinal cell populations. Results correspond to expected outcomes and are similar to previous data in normal and degenerate retina. Results in degenerate retinal tissues reveal substantial hypertrophy and expansion of Müller cell populations in degenerate retina (Jones et al., 2003, 2005, 2006; Marc and Jones, 2003; Marc et al., 2003, 2007; Jones and Marc, 2005).

The GABA antibody was used to detect populations of amacrine cells (Grunert and Wassle, 1990; Wulle and Wagner, 1990; Crooks and Kolb, 1992), including the AII amacrine cells, some horizontal cells in the central retina (Kalloniatis et al., 1996), and a small population of bipolar cells (Martin and Grunert, 1992). GABA labeling was also used in degenerate retinas as a rapid identifier of remodeling retinas, as processes extending outside of the normal lamination patterns of retina are easily identified (Jones et al., 2003). Labeling corresponded to expected outcomes in normal and degenerate retina identical to that observed in other studies (Jones et al., 2003, 2005, 2006; Marc and Jones, 2003, Marc et al., 2003, 2005a, 2007, 2008; Jones and Marc, 2005).

Rod opsin antibodies have been routinely used to reveal the presence and extent of rod opsin in the normal and degenerate retina (Hicks and Molday, 1986; Marc et al., 2008). The antibody reveals monomers and dimers of rhodopsin at ~35 and 70 kDa on Western immunoblot analysis of isolated bovine outer segments (Molday and

MacKenzie, 1983). Rod opsin immunoreactivity in this study corresponded to expected outcomes as rod photoreceptors degenerated.

Antibody to mGluR6 was used to visualize mGluR-immunoreactive puncta and define the limits of ON-bipolar cell dendrites in the the outer plexiform layer (Vardi et al., 2000). Specificity was evaluated by Gargini et al. (2007) through Western blots with recognized bands disappearing through antibody preabsorption with the synthetic peptide antigen. Additionally, immunolabeling reveals identical punctate structures in our data as those reported by Li et al. (2004) in normal tissues. Immunoreactivity in degenerate retina was similar to that observed in Strettoi and Pignatelli (2000) and Strettoi et al. (2002).

The CRALBP antibody was used to define Müller cell populations. The antibody shows a single band of $\sim$35 kDa on Western blots of rabbit retinal extracts (Anderson et al., 1986; Sarthy and Bickoff, 1996) and has been commonly used to define Müller glia in normal (Bunt-Milam and Saari, 1983) and retinal degenerate tissues (Marc et al., 2008). CRALBP labeling in this study was as expected in the normal tissues and serves as an excellent marker for Müller cells in the complex pathologies in degenerate retina.

PKCα is a specific marker for rod bipolar cells and a small population of cholinergic amacrine cells (Haverkamp and Wässle, 2000; Peng et al., 2000). It was used in this study to specifically examine rod bipolar cells and their dendritic and axonal arbors identical to those in normal (Haverkamp and Wässle, 2000) retina, but exhibiting altered morphologies in degenerate tissues. On sodium dodecyl sulfate-polyacrylamide gel electrophoresis (SDS-PAGE) immunoblot, this antibody shows an 80-kDa polypeptide band with a minor band at $\sim$45 kDa in rat brain extract.

Cone arrestin was used to visualize cone photoreceptors from the pedicles to the outer segments in normal and degenerate retina. Cone photoreceptor structures in normal rabbit retina were similar to those illustrated in Hendrickson et al. (2009), but by 40 weeks in the degenerate retina, only faint, punctate immunoreactivity could be seen in cone photoreceptors. The antibody shows a $\sim$57-kDa band on Western immunoblot analysis of isolated bovine retina according to the manufacturer (#178605-200UG, Merck Biosciences, Darmstadt, Germany).

Calbindin mouse monoclonal antibodies have been commonly used to show both horizontal cells and a subpopulation of cholinergic amacrine cells and their processes (Haverkamp and Wässle, 2000). Calbindin has also been used to study alterations in horizontal cell morphology in retinal degenerations (Fariss et al., 2000) and showed similar results in this study. The antibody stains the ^{45}Ca binding spot of calbindin-D (MW = 28,000, pI = 4.8) in a two-dimensional immunoblot according to the manufacturer, and in Western blots the antibody recog-

nizes a single 28-kDa band in rabbit cerebellum (Celio et al., 1990).

LWS red/green opsin has been used to visualize LWS cones (Haverkamp et al., 2005; Fischer et al., 2007) and specifically labels red/green cone outer and inner segments (Wang et al., 1992; Otani et al., 2004; Yan et al., 2010). The LWS red/green opsin antibody recognized red/green opsin with band of $\sim$40 kDa, but not blue opsin in mouse retinal extracts from the manufacturer (Chemicon/Millipore, Temecula, CA). As expected, the antibody revealed red and green cones in normal human and rabbit tissues. In degenerate human and P347L rabbit tissues, punctate staining was seen early in degeneration; in tissues in which cones were degenerated, no labeling was observed.

GS is commonly used to reveal Müller glia (Haverkamp and Wässle, 2000) and recognizes a single 45-kDa band on Western blots in sheep brain from the manufacturer. Immunoreactivity in this study was identical with previous results with the exception of increased levels in Müller cells engaging in Müller cell seal formation (Jones et al., 2003).

Electron Microscopy (EM)

Rabbit tissues were postfixed in 1% buffered osmium tetroxide with 1.5% potassium ferrocyanide. Tissue was then embedded in Epon resin, sectioned at a thickness of 90 nm, and collected on single-slot grids with a carbon-coated formvar film. Sections were poststained with uranyl acetate followed by lead citrate. Large-scale transmission electron microscopy (TEM) was then performed, creating EM mosaics as previously described (Anderson et al., 2009).

RESULTS

The objective of this work was to compare the course of retinal degeneration in the TgP347L rabbit with that in human adRP. As in human retina, progressive rod-specific degeneration in the TgP347L rabbit leads to complete loss of rods by 40 weeks, but permits isolated survival of deconstructed cones. Importantly, the presence of morphologically deconstructed cones prevents the onset of gross remodeling and, of substantial import, appears to preserve iGluR-coupled signaling to horizontal and bipolar cells. Also similar to human retina, survivor bipolar cells, amacrine cells, and horizontal cells show evidence of neurite de novo sprouting and altered signaling by reprogrammed IGluR expression.

Basic disease progression
ERG

To evaluate retinal function in the TgP347L rabbit, ERGs were recorded with various stimulus intensities
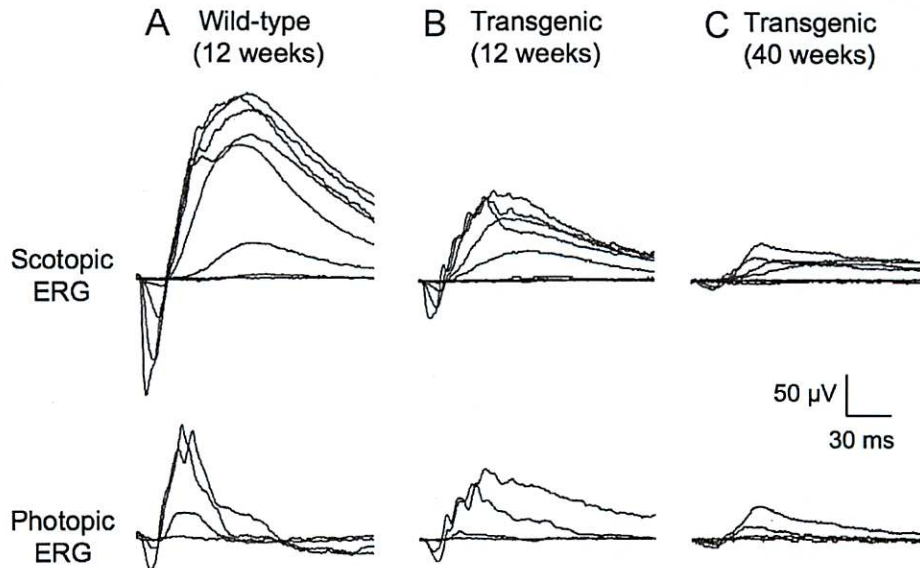
Figure 1. A–C: Electroretinograms (ERGs) recorded from 12-week-old wild-type (A) and 12- (B) and 40-week-old (C) TgP347L transgenic rabbits. Upper trace: scotopic ERGs elicited by eight different stimulus intensities ranging from -4.8 to 2.2 log cd s m^{-2}. Lower trace: photopic ERGs elicited by four different stimulus intensities ranging from -0.8 to 2.2 log cd s m^{-2} on a rod-suppressing white background of 1.3 log cd m^{-2}.

under scotopic and photopic conditions from 12-week-old wild-type (Fig. 1A) and 12- (Fig. 1B) and 40-week-old (Fig. 1C) transgenic rabbits. When compared with 12-week-old wild-type rabbit, the ERG amplitudes of 12-week-old Tg rabbit were clearly reduced, and the reduction of scotopic ERGs was more severe than that of photopic ERGs. At 40 weeks, the maximal a-wave amplitudes dropped below 10 μV for both scotopic and photopic ERGs. In addition, when rod a-wave was isolated by waveform subtraction of photopic ERG from scotopic ERG, the maximal rod a-wave amplitude was nearly undetectable in 40-week-old Tg rabbits. These results indicated a rod-dominant, progressive photoreceptor degeneration in the TgP347L transgenic rabbits, with rod function nearly lost by 40 weeks.

Electron microscopy

Early in retinal degeneration, at 12–16 weeks in the TgP347L rabbit, overall photoreceptor structure appeared more or less intact, with the exception of some disorganization in the outer segments of photoreceptors; large portions of outer segments were breaking off, appearing to remain in the subretinal space. Most notable, however, were large numbers of small vesicular rod photoreceptor outer segments that broke off and appeared as a rhodopsin "froth" or large concentrations of small rhodopsin-filled vesicles in the outer retina above and surrounding the remaining outer segments of the photoreceptors in the subretinal space (Fig. 2A–C).

(Fig. 3 B, E, F)

In the 40-week TgP347L rabbit retina, truncated cone synapses from remnant cone photoreceptors were also identifiable and are representative of existing photoreceptor contacts as the sole remaining synapses with no rod synaptic contacts identifiable (data not shown).

Marked variations in Müller cells with remarkably high concentrations of polyribosomes in immediately adjacent Müller cells were found beginning early in the 16-week animal. By 40 weeks in the TgP347L rabbit, the proportion of Müller cells demonstrating massive upregulation of protein and presumably polyribosomes was significantly greater (see Fig. 4A–C). This upregulation of apparent protein synthesis in Müller cells suggests large changes in protein expression profiles. Müller cells thus appear to alter their normally homogenous small-molecular signatures as well as protein expression profiles, observed in the micromolecular signals (see Figs. 4D, 8B, 10A,B), macromolecular immunohistochemistry (see Fig. 9C,F), and the polyribosome and protein upregulation (see Fig. 5A–C), resulting in substantial Müller cell to Müller cell heterogeneity.
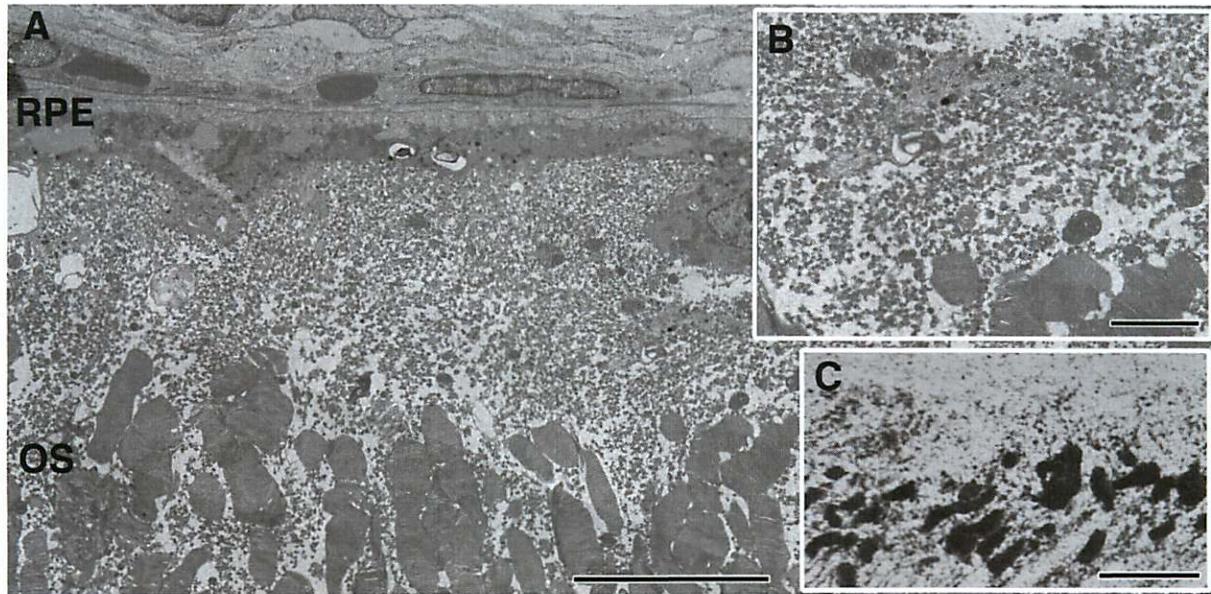
Remodeling and metabolic stress
CMP

CMP allows acquisition of multidimensional small-molecular signatures that can then be segmented by classifier algorithms, revealing natural cellular classes (Marc and Cameron, 2002; Marc and Jones, 2002).

Both TgP347L rabbit and human adRP retinal tissues from humans were probed with IgGs targeting L-asparate,

Figure 2. TEM of the subretinal space in a 16-week TgP347L rabbit. **A:** Debris in the subretinal space composed of 40–300-nm vesicles (inset **B**) above and in between the photoreceptor outer segments (OS). The vesicles are immunoreactive for rod opsin in and around the existing photoreceptor outer segments (inset **C**). For abbreviations, see list. Scale bar = 10 μm in A,C; 2.0 μm in B.

L-glutamate, glycine, L-glutamine, glutathione, GABA, and taurine. All retinal tissue can be segmented into superclasses or classes by using combinations of probes, and select signal triplets are mapped as rgb images for visualization. Many classes of neurons and glia are easily visualized with γGE :: rgb mapping, such as photoreceptors, bipolar cells, GABA+, and glycine+ amacrine cells and ganglion cells. Alternatively, τQE :: rgb visualization allows retinal pigmented epithelium and Müller cells to be observed independent from all other cell classes.

We documented progressive photoreceptor loss in the TgP347L rabbit retina over the course of 40 weeks, with early indications of retinal circuit revision and overall retinal remodeling consistent with observations in other models (Banin et al., 1999; Peng et al., 2000; Strettoi and Pignatelli, 2000; Jones et al., 2003, 2005; Marc and Jones, 2003; Strettoi et al., 2003; Jones and Marc, 2005). The rabbit TgP347L model of retinal degeneration demonstrates, as in human retina, progressive rod-specific degeneration in an erratic distribution over the retina, with rod degeneration in the most affected areas essentially complete by approximately 40 weeks.
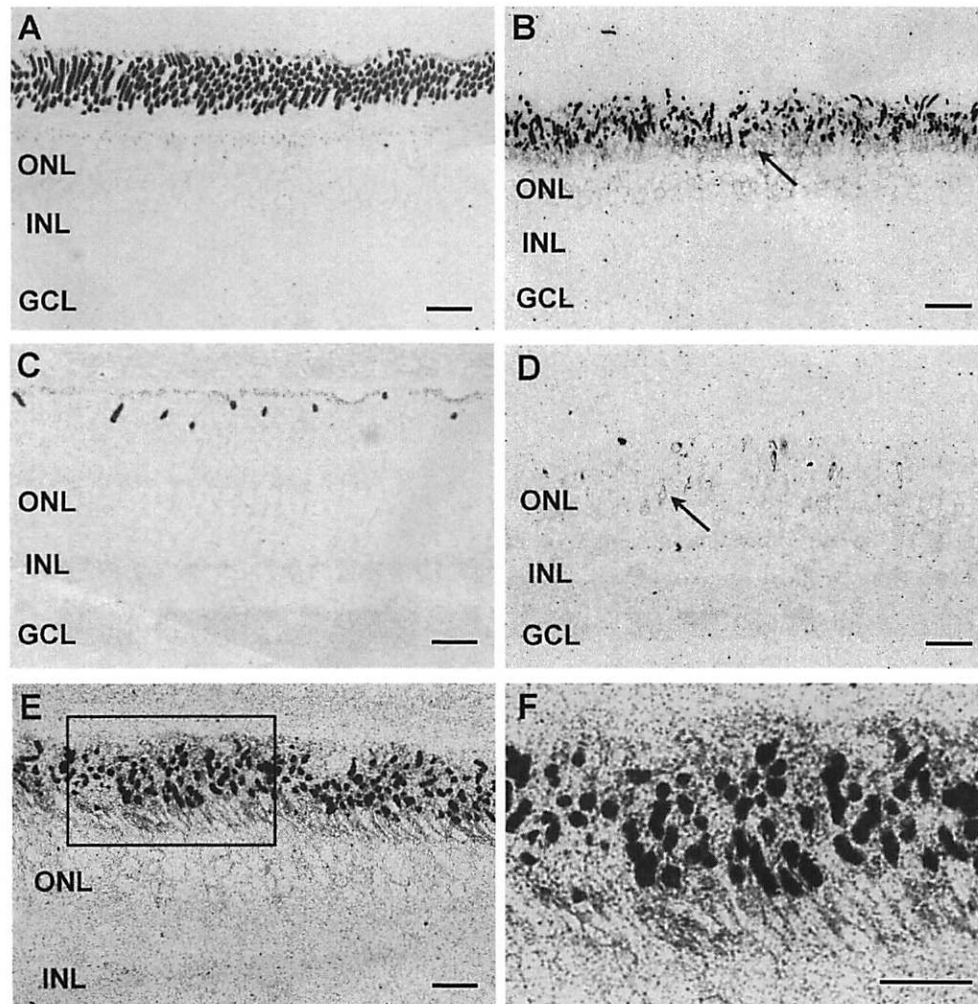
12 weeks

At 12–16 weeks in the TgP347L rabbit retina, many rod photoreceptors were lost, and remaining cone photoreceptors exhibited early evidence of photoreceptor stress as isolated cone photoreceptors exhibiting spikes in taurine signals (see Fig. 5A). Alterations in the CMP sig-

natures of Müller cells were also observed in the glutamine, glutamate, and glutathione signals, indicating isolated changes or alterations in the metabolism of immediately adjacent Müller cells (see Fig. 5B–D). Glutathione concentrations also varied independently from Müller cell to Müller cell, implying that retinal stress pathways are not isolated to photoreceptor cells. Cluster analysis of adjacent Müller cell end-feet revealed multiple metabolic states through glutamine, glutamate, and glutathione content (see Fig. 7). This did not occur in normal retina. Even in regions where rod photoreceptors are present at close to normal numbers, sprouting of amacrine cells had begun. Both glycinergic and GABAergic amacrine cells sent dendritic profiles toward and into the photoreceptor cell layer (see Fig. 5E,F). Glutathione appeared to be the first molecular signal altered in Müller cells in regions of retina that still possessed nearly normal numbers of rod photoreceptors (see Fig. 5D). Even at this relatively early stage of retinal degeneration with photoreceptor cell nuclei being present at three to four cells thick, Müller cell signals were radically altered, suggesting focal responses to cell stress. It should be noted that this pattern of glutamate, glutathione, and glutamine immunoreactivity is common throughout the retina with many regions of early degenerative retina showing large spikes (arrows in Fig. 5D) in concentrations of these amino acids in Müller cells. Photoreceptors in these areas demonstrated other indicators of cell stress including delocalized rod opsin (Fig. 3B,E,F) and delocalized cone opsin (Fig. 3D).

The Journal of Comparative Neurology | Research in Systems Neuroscience   7

ID: **jaishankarn** | Black Lining: **[ON]** | Time: **18:02** | Path: N:/3b2/CNE#/Vol51913/110135/APPFile/JW-CNE#110135

Figure 3. Opsin immunoreactivity. **A,B:** Rod opsin in (A) control and (B) 12-week TgP347L rabbit retinas. The TgP347L rod outer segments are shorter and disorganized, and show substantial rod opsin mislocalization to the inner segments (arrow). **C,D:** LWS opsin in (C) control and (D) 12-week TgP347L rabbit retinas. Cone outer segments are sparse and spot-like in the TgP347L animals and show mislocalization to the inner segments and cone photoreceptor cell bodies (arrow). **E:** Rod opsin debris in a 16-week TgP347L rabbit retina demonstrating fine ∼20–40-nm-diameter particulate rod opsin. **F:** Magnified view of inset box in E shows rod opsin in the outer segments as well as delocalized rod opsin in the inner segments and membrane surrounding the photoreceptor cell bodies. For abbreviations, see list. Scale bar = 20 μm in A–D; 30 μm in E,F.
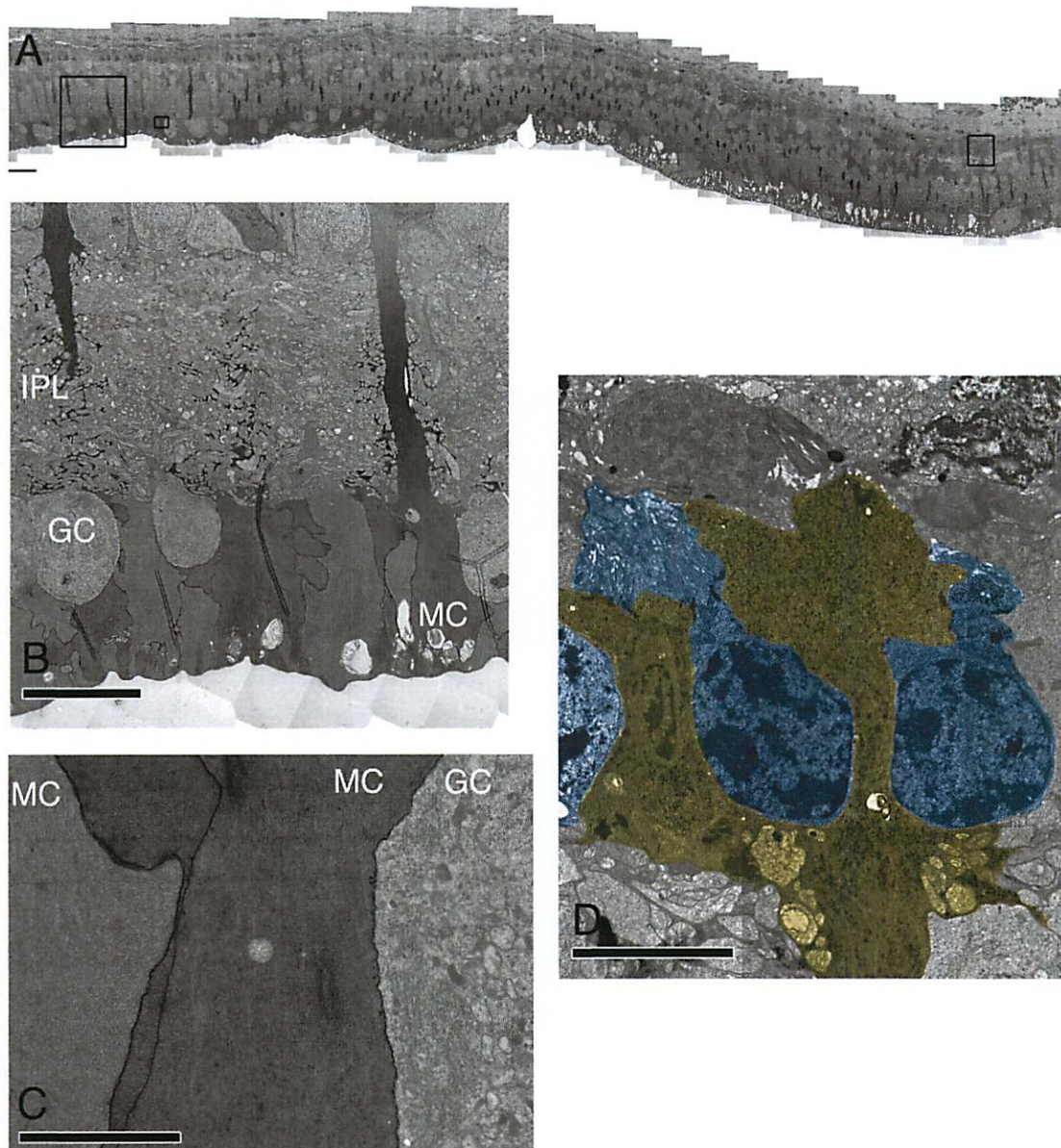
40 weeks

Sprouting of amacrine cells in the TgP347L rabbit retina was more common at 40 weeks, with amacrine cell processes approaching the remnant subretinal space and running along the underside of the formed Müller cell seal F6 (Fig. 6E,G,H). These findings closely resemble the mechanism of retinal degeneration and remodeling in human RP and other mammalian models of RP (Peng et al., 2000; Strettoi and Pignatelli, 2000; Jones et al., 2003; Marc and Jones, 2003; Marc et al., 2003, 2005a, 2007, 2008) and mirror our findings of dendritic sprouting in examples of F8 human adRP (see Fig. 8C–F).

At 40 weeks in the TgP347L rabbit retina, Müller cells showed varying taurine and glutamine signals in a patchy fashion. These variations became more common throughout the retina at times later in the degenerative process, with taurine and glutamine levels in these cells spiking whereas minor changes in GABA levels could be seen to subtly rise in apical or proximal portions of Müller cells that were forming the Müller cell seal (Jones and Marc, 2005) (Fig. 6E). These changes in taurine, glutamine, and glutamate (Fig. 6A–C) may indicate Müller cells undergoing transformations and possible attempts to osmoregulate. Interestingly, at later stages in the disease, glutathione content in Müller cells normalized to some degree, exhibiting less dramatic variation in Müller cells undergoing Müller cell seal formation (Fig. 6D). The use of τQE::rgb visualization allows simultaneous visualization of

Figure 4. TEM of the TgP347L rabbit retina at 40 weeks. **A:** Image mosaic of over 5,000 individual EM images, each at 5,000× magnification, 2.18 nm/pixel. The dark Müller cell profiles represent regional fluctuations in polyribosome and protein upregulation. **B:** An enlarged region of A demonstrating the variation in polyribosome upregulation. Note the strong variation in density of neighboring Müller cell endfeet (MC). **C:** An enlarged region of A illustrating increased cytosolic polyribosome content in MCs next to a ganglion cell (GC) as well as enhanced protein content in the cell membrane of the MC. **D:** Müller cell seal formation between remnant photoreceptor cells (blue). For abbreviations, see list. Scale bar = 40 µm in A; 20 µm in B; 10 µm in C,D.

Müller cells and RPE independent from all other cell classes. L-glutamate labeling in combination with taurine demonstrated three surviving cones protruding above the Müller cell seal, whereas variations in the Müller cell signatures could be observed, suggesting pathological heterogeneity in Müller cell metabolism. Interestingly, although most other signatures were the same, the presumptive macrophage in the retina proper had much higher glutamine and glutathione signals (Fig. 6B,D,H).

Overall, normal-appearing lamination of excitatory and inhibitory cell populations in the TgP347L rabbit retina was present at 40 weeks, but amacrine cell classes could be observed sprouting as fine filamentous processes (Fig. 6E,F). Examination of rod photoreceptors in the 40-week TgP347L rabbit, even in regions where there is significant rod photoreceptor survival, revealed substantial photoreceptor cell stress, as evidenced by rod and cone opsin delocalization into the membrane surrounding the cell
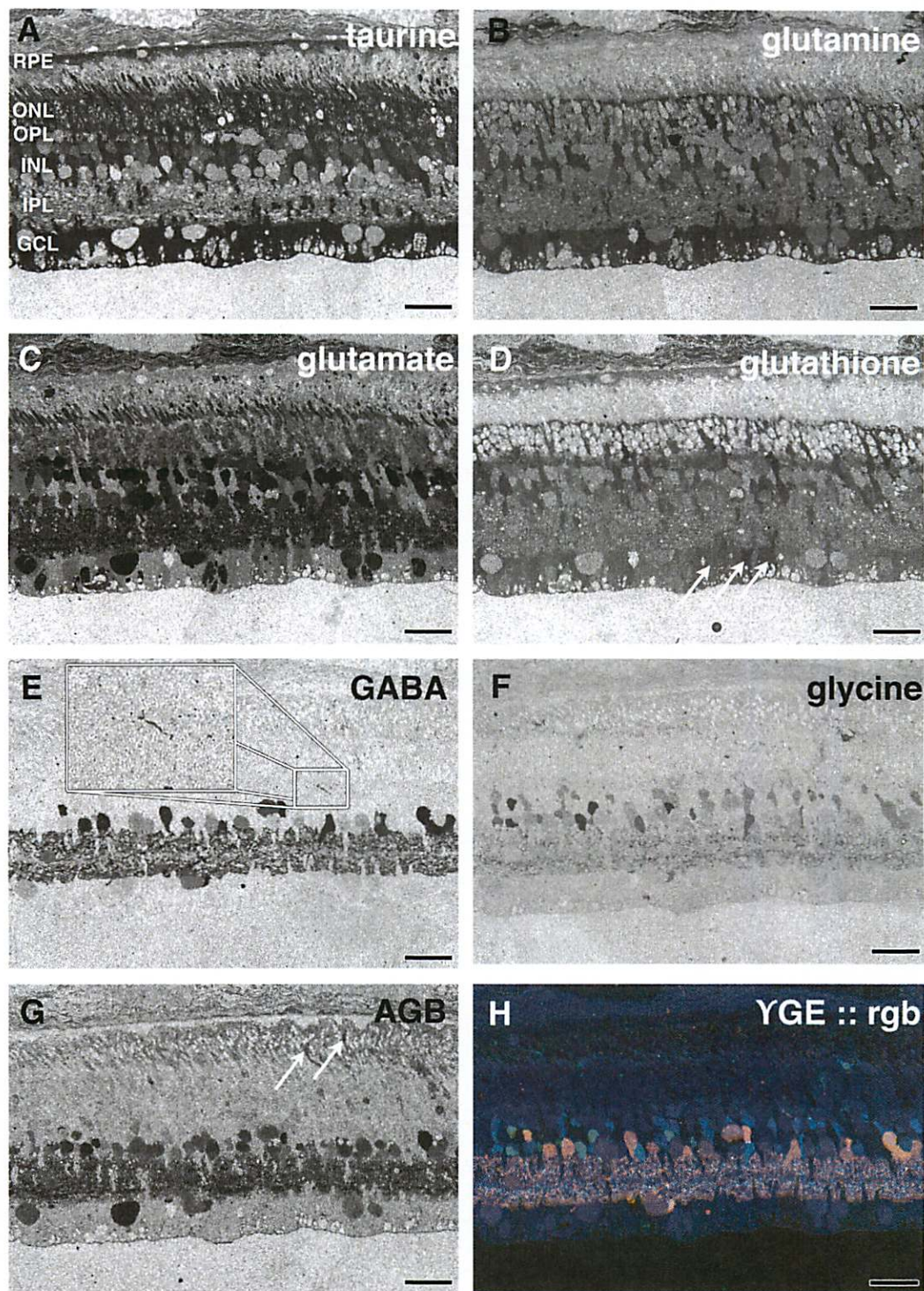
Figure 5. CMP of 16-week old TgP347 rabbit retina. A–H: (A) taurine, (B) glutamine, (C) glutamate, (D) glutathione, (E) GABA, (F) glycine, (G) AGB, and (H) γGE :: rgb mapping. Arrows in D indicate Müller cell end feet with varying glutathione levels. Inset in E shows amacrine cell neurite in the outer plexiform layer. Arrows in G show permeation of AGB into photoreceptors. For abbreviations, see list. Scale bar = 30 μm in A–H.

body (Fig. 3B,D). Finally, some evidence of presumed macrophage invasion (Fig. 6, inset) into the sub-RPE/photoreceptor layer from early to late stages of retinal photoreceptor degeneration (Fig. 6A–H) was observed, suggesting a possible mechanism for post-photoreceptor cell detritus removal from the subretinal space.
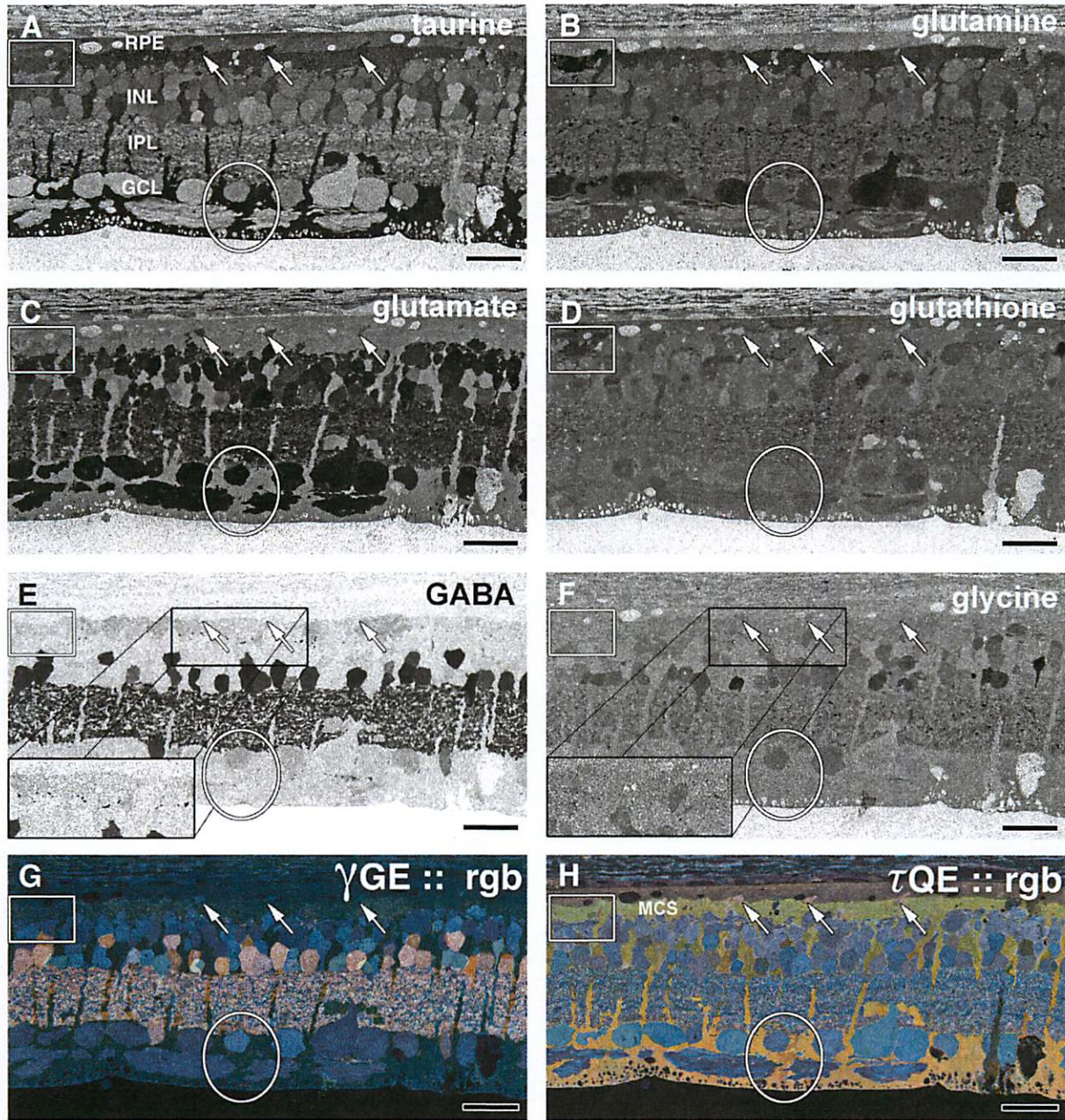
Figure 6. CMP of 40-week old TgP347L rabbit retina. **A:** Taurine. Arrows indicate small taurine+ survivor cones at the border between the RPE and the Müller cell seal (MCS). **B:** L-glutamine. Glutamine signals are elevated in Müller cells that form the distal seal. Presumed macrophages show high concentrations of glutamine (box). **C:** L-glutamate. Reduced numbers of glutamate+ bipolar cells suggest cell death. **D:** Glutathione. Müller cells show variability in glutathione levels (oval). Presumed macrophages show high concentrations of glutamine (box). **E:** GABA. Increased GABA expression in Müller cells and anomalous neurites from GABAergic amacrine cells running underneath the Müller cell seal (rectangle). **F:** Glycine. **G:** γGE :: rgb visualizes photoreceptor, bipolar cell, GABA+ and glycine+ amacrine cells and ganglion cell superclasses. **H:** τQE :: rgb visualizes retinal pigmented epithelium and Müller cells. Three surviving cones (arrows) protrude above the Müller cell seal. Variation in the Müller cell signatures is evident (oval). For abbreviations, see list. Scale bar = 30 μm in A–H.

CMP hman RP

Human tissues from a 29-year-old patient with adRP were also examined (Fig. 8B,D,F). These samples of human cone-sparing RP retina allowed for comparison of small-molecular signals and the AGB response properties at a time point that coincided with the 40-week TgP347L rabbit retina, in which most rod photoreceptors (90–100%) were lost in a regional distribution, and, notably,
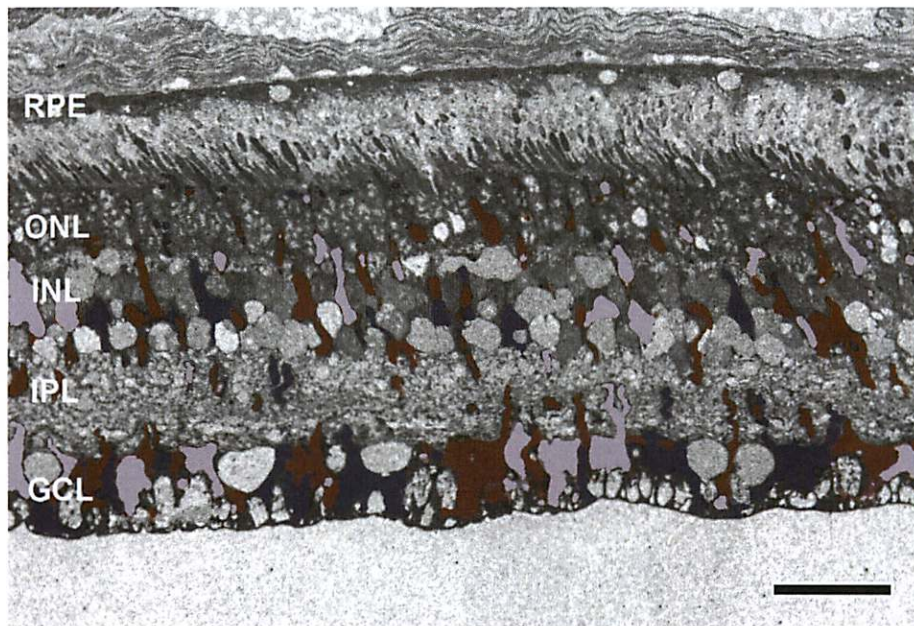
Figure 7. Refined theme map derived from clustering of Müller cells in the 12-week TgP347L Tg rabbit overlaid on the taurine channel revealing three separate metabolic classes in Müller cells representing distinct pathological metabolic states. For abbreviations, see list. Scale bar = 30 μm.

the remaining cones resembled those found in the TgP347L rabbit. These tissues bore remarkable similarities to the 40-week TgP347L rabbit, with identical findings of glycinergic and GABAergic amacrine cell sprouting, seen most clearly in the GABA (Fig. 8C,D) and glycine signals as processes were seen departing from the normal lamination of the IPL. Glial seal formation was identical in both the TgP347L rabbit and the adRP human retina in areas bereft of any remaining photoreceptors, although in regions where there was incomplete loss of photoreceptors (Fig. 8A,B), Müller cells could be seen undergoing hypertrophy and migrating up through the remaining photoreceptors to initiate the Müller cell seal in both human and TgP347 L rabbit.

However, as in the TgP347L rabbit, the presence of rod or cone photoreceptors in the human RP retina appeared to attenuate gross retinal remodeling exemplified by neuronal translocation to other regions of the retina. Additionally, Müller cell signatures were altered in glia that were immediately adjacent to one another (oval), demonstrating heterogeneous responses to the degenerative retinal microenvironment. This variation of metabolic programming among a population of cells that normally expresses homogeneous metabolic envelopes is aberrant in both the TgP347L rabbit and human adRP retinas (Fig. 8A,B). Glycinergic and GABAergic amacrine cells also began to sprout novel processes, illustrating the plastic nature of the remodeling retina (Fig. 8C,D and red and

green channels in Fig. 8E,F). γGE :: rgb mapping of the rabbit 347L and human adRP retinas, respectively (Fig. 8E,F), demonstrated combinations of photoreceptor, bipolar cell, and ganglion cell superclasses while revealing aberrant GABA+ and glycine+ amacrine cells. The sprouting of both GABA+ and glycine+ amacrine cell processes could also be visualized in the red and green channels of the γGE :: rgb image, with processes from both cell classes appearing outside their normal lamination (Fig. 8E,F). Finally, the TgP347L rabbit exhibited populations of bipolar cells that indicate altered reprogramming, with populations of bipolar cells changing their signaling from ON responses to OFF responses (Marc et al., 2007).

Macromolecular immunohistochemistry

In addition to the probes for small-molecular signals, we employed serial antibodies against macromolecular targets, rhodopsin 1D4, LSW red/green opsin, and CRALBP in thin section immunohistochemistry, and calbindin, GS, PKCα, cone arrestin, mGluR6, and CRALBP in traditional confocal microscopy.

By 12 weeks in the TgP347L rabbit, both rod (Fig. 3B,E,F) and cone (Fig. 3D) opsin delocalization were observed. The former was described by Strettoi and colleagues (Strettoi and Pignatelli, 2000; Strettoi et al., 2002), and both are indicators of photoreceptor cell stress.

By 40 weeks, substantial alterations in the architecture had occurred in the TgP347L rabbit retina. DAPI labeling
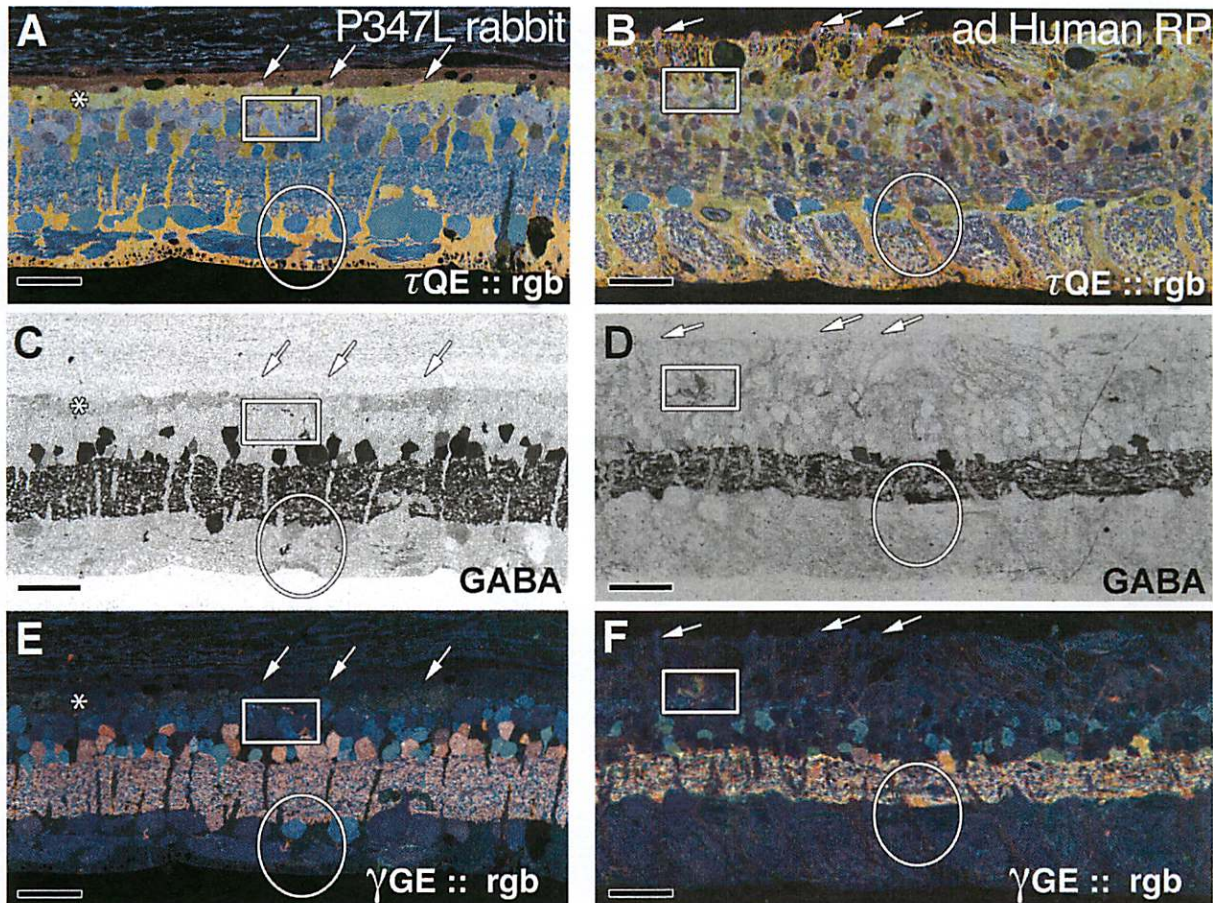
Figure 8. A: τQE :: rgb visualization in the TgP347L rabbit retina. The Müller cell seal in this region is almost complete. Four to five remnant cone photoreceptors are evident along with a presumed macrophage (to the right of the asterisk). Isolated surviving cones can be observed embedded in a well-formed Müller cell seal (arrows). **B:** Altered Müller cell signatures (oval) are observed in both the TgP347L rabbit (A) and in the ad Human RP retina, in which formation of the Müller cell seal is not complete. Instead, alterations in Müller cell signatures are present along with hypertrophy of Müller cell processes in and around the remnant photoreceptors. **C,D:** γ-Aminobutyric acid (GABA) labeling in the TgP347L rabbit retina (C) and human adRP retina (D) with sprouting of amacrine cell processes observed outside of the normal lamination of the IPL (box). **E,F:** γGE :: rgb visualization of the rabbit 347L (E) and human adRP (F) retinas demonstrating photoreceptor, bipolar cell, GABA+, and glycine+ amacrine cells and ganglion cell superclasses. Sprouting of both GABA+ and glycine+ amacrine cell processes can be visualized in the red and green channels with processes from both cell superclasses appearing outside their normal lamination. Scale bar = 30 μm in A–F.

demonstrated thinning of the photoreceptor/bipolar cell layers in the TgP347L rabbit retina versus normal wild-type retina (Fig. 9A,B). GS became dramatically upregulated in a mosaiced fashion in the degenerate TgP347L rabbit retina, demonstrating altered metabolic envelopes in Müller cells (Fig. 9C), whereas rod opsin immunoreactivity in regions of photoreceptor cell loss had been largely eliminated, with only punctate labeling in the remnant subretinal space evident (Fig. 9D). Cone arrestin in the 40-week rabbit retina produced only punctate labeling in surviving cone inner segments (data not shown), demonstrating substantial loss of cone photoreceptors. LSW1 cone opsin immunoreactivity in the TgP347L rabbit was reduced to slight labeling and delocalization through-

out the cell membrane (Fig. 3D) or was eliminated entirely, as observed in the human retina (Marc et al., 2007), whereas calbindin immunoreactivity of the TgP347L rabbit tissue demonstrated horizontal cell body hypertrophy along with substantial aberrant sprouting of horizontal cell processes into the IPL (Fig. 9B,E). The large number of horizontal cell terminals in the IPL also appeared to demonstrate that significant numbers of horizontal cells were contributing to sprouting into the IPL.

Additionally, calbindin immunoreactivity appeared to intensify labeling in the degenerate retina compared with wild-type retina, although this may simply reflect hypertrophy and z-axis superimposition of horizontal cell membrane in the confocal preparation. PKC labeling
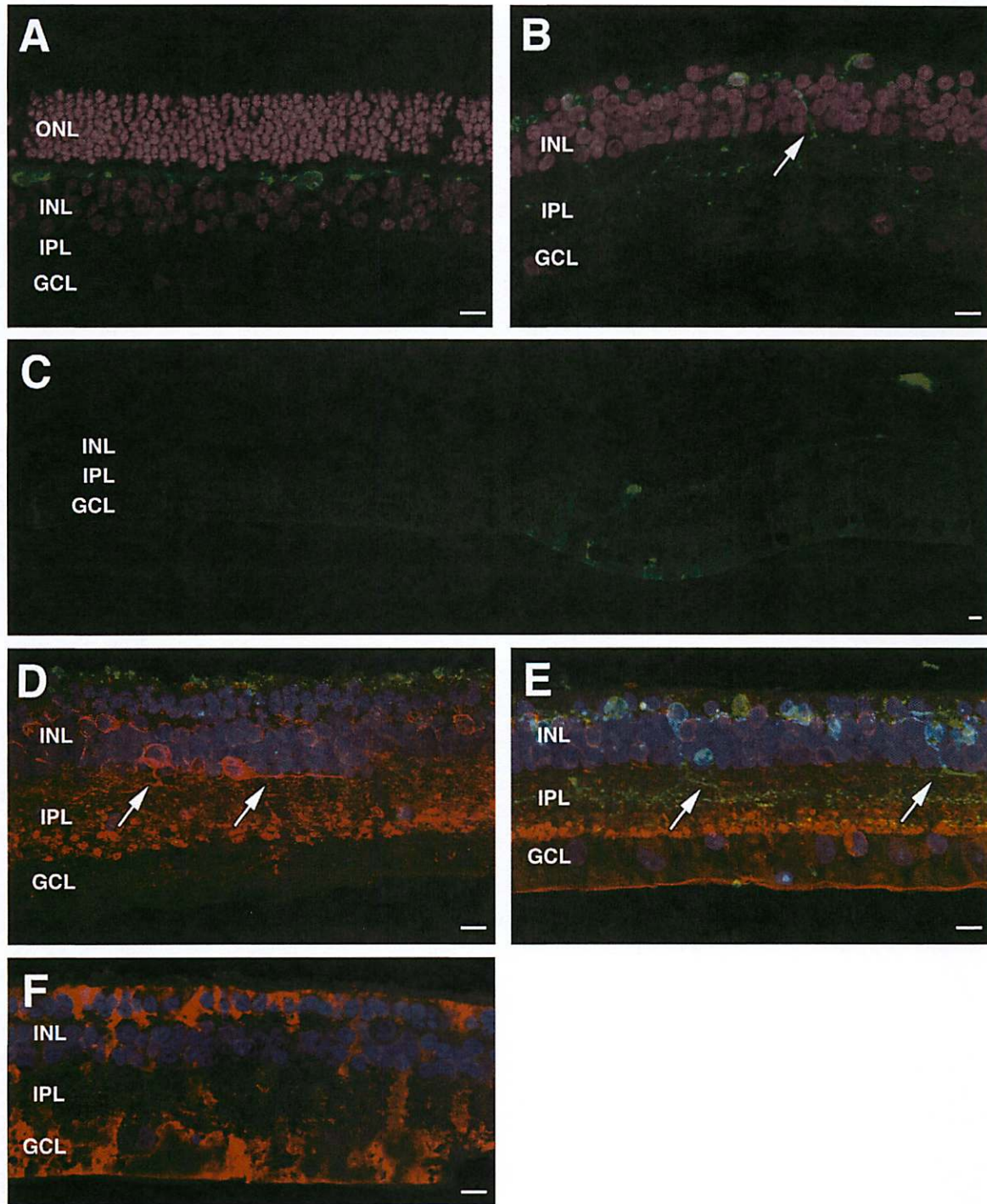
Figure 9. Confocal microscopy of WT and 40-week TgP347L retinas. **A,B:** DAPI (magenta) + calbindin (green) images from wild-type retina (A) and DAPI (magenta) + calbindin (green) images from TgP347L rabbit (B) demonstrating horizontal cell remodeling in the degenerate retina. **C:** Mosaiced GS expression in TgP347L retina. **D:** Maximal projection image of PKC (red), Rho 1D4 (green), and DAPI (blue) demonstrating reduced rhodopsin immunoreactivity and new rod bipolar cell axons projecting along the border of the IPL (arrows). **E:** Maximal projection image of PKC (red), calbindin (green), and DAPI (blue) demonstrating calbindin labeling in horizontal cells with altered PKC expression. Horizontal cell processes project into the IPL (arrows). **F:** CRALBP immunostaining of Müller cells demonstrating glial hypertrophy and envelopment of remnant bipolar cells and photoreceptors, forming the intial Müller cell seal. For abbreviations, see list. Scale bar = 10 μm in A–F.

demonstrated a reduced cohort of rod bipolar cells along with altered stratification of terminal cell endings. In maximal projection images, PKC immunoreactivity revealed bipolar cell axons that sprouted and ran horizontally through the retina along the border of the IPL (Fig. 9D,E). CRALBP immunostaining revealed variation in the labeling of CRALBP as well as the hypertrophic nature of Müller cells and formation of the Müller cell seal in the remnant subretinal space in the degenerate TgP347L rabbit retina (Fig. 9F). It should be noted that Müller cell hypertrophy is a common theme in retinal degenerations regardless of primary insult (Jones et al., 2003; Marc et al., 2003; Jones and Marc, 2005). mGluR6 immunoreactivity also demonstrated delocalization from the former dendritic processes down into the IPL in a punctate fashion, as observed by Strettoi and colleagues (Strettoi and Pignatelli, 2000; Strettoi et al., 2002, 2003) (data not shown).

Reprogramming

Three major types of bipolar cells have been described in mammals: ON cone bipolar cells, OFF cone bipolar cells, and rod bipolar cells (Wässle and Boycott, 1991). CMP reveals two major classes of bipolar cells, ON cone bipolar cells and a complex of rod and OFF cone bipolar cells (Kalloniatis et al., 1996; Marc et al., 1998b). An additional toolset that can be brought into the CMP armamentarium is AGB probing of glutamate channel permeation. AGB both contributes functional data to CMP and acts as an additional discriminand (Marc, 1999a; Marc and Jones, 2002), reliably demonstrating and supporting data from physiological experiments showing that ON bipolar cells utilize metabotropic GluRs and are thus KA insensitive (Slaughter and Miller, 1981, 1983; Karschin and Wässle, 1990; Yamashita and Wässle, 1991; Sasaki and Kaneko, 1996). OFF bipolar cell responses were substantial in response to KA and labeled strongly with AGB, whereas rod bipolar cells showed no labeling after KA administration (Marc, 1999c). Thus, through the application of KA + AGB, we can visualize neuronal classes including bipolar cell classes presenting with AMPA/KA receptor pharmacological phenotypes (Marc, 1999c).

Similar to findings in the mouse (Marc et al., 2007), the rabbit exhibits apparent phenotypic revisions of bipolar cell classes in response to photoreceptor cell death that eliminates functional mGluR6 and iGluR expression, effectively converting rod and OFF bipolar cells to an ON F10 F11 bipolar cell phenotype (Figs. 10A–F, 11A–C).

Excitation mapping with KA activation followed by GBE :: rgb mapping segments the entire retina into three kinds of bipolar cells. Pure blue cells are rod bipolar cells; magenta cells are ON cone bipolar cells coupled to glycinergic amacrine cells; and cyan cells are OFF bipolar cells that express AMPA receptors. In the normal retina across
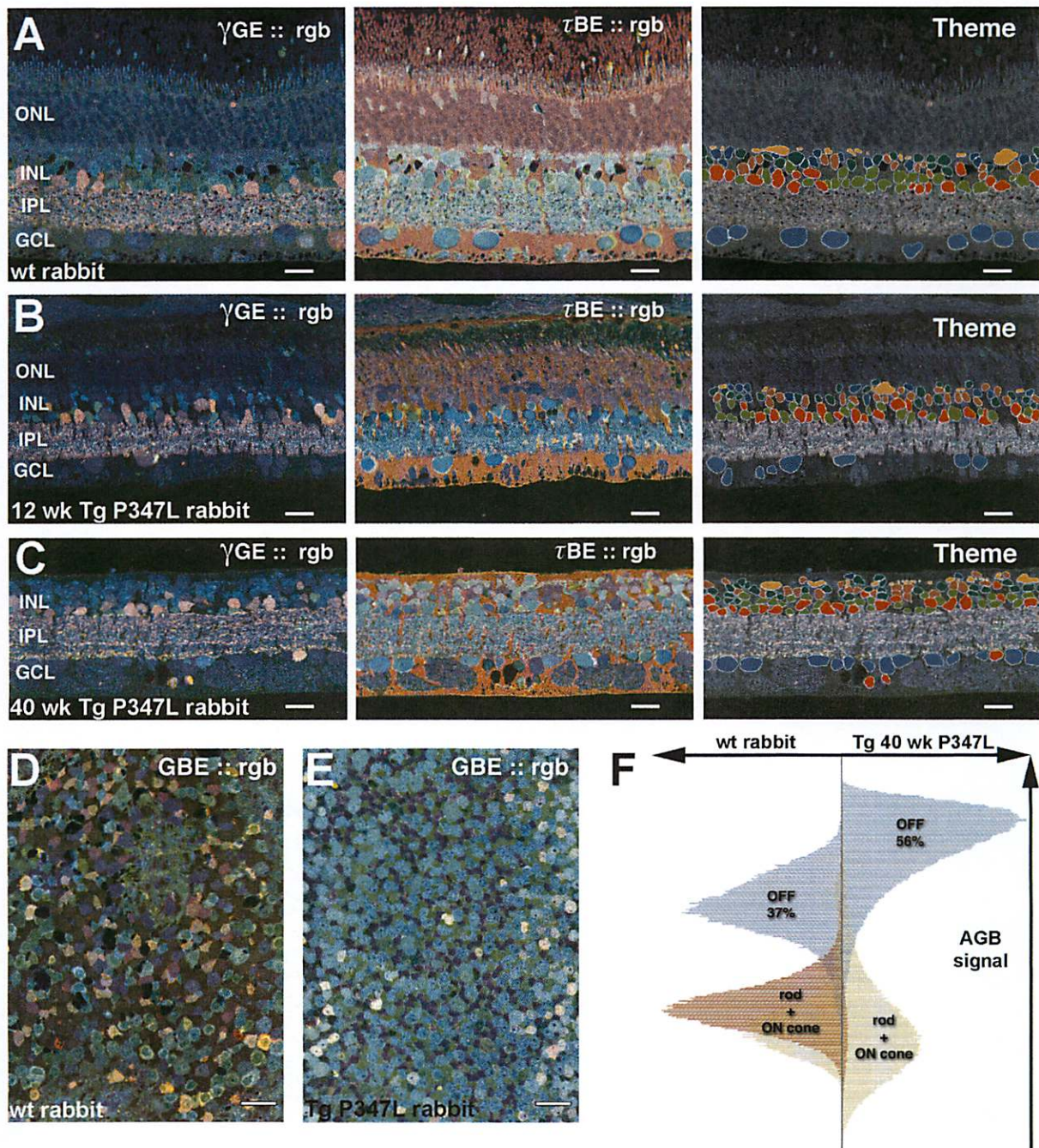
species (Marc et al., 2007), about 30–40% of bipolar cells are classified as OFF by this criterion (wild type [WT] in Fig. 10D). In the 40-week TgP347L rabbit, the fraction of KA-responsive bipolar cells increased to over 56%, whereas the fraction of identifiable rod bipolar cells decreased from 30% to 1% (TgP347L in Fig. 10E). The classical rod bipolar cell phenotype was essentially absent from the TgP347L retina.

The demonstration of neurite sprouting and likely retinal reprogramming by alterations in iGluR expression is the most significant finding in survivor bipolar cells and horizontal cells in the TgP347L rabbit retina. (Figs. 9B,D,E, 10B,C). By 40 weeks, the TgP347L rabbit retina exhibited regions of degeneration and remodeling (Figs. 9B,C,D,E, 11A–C) and marked phenotypic revision of bipolar cells as they downregulateed iGluR and mGluR6 expression, recapitulating observed results in rodent and human retinal degenerations (Marc et al., 2007). After photoreceptor cell loss in the TgP347L rabbit, as in human and rodent models of RP, bipolar cells lost their iGluR-mediated responses, whereas amacrine cells and ganglion cells in the same retina maintained iGluR-mediated activity.

The finding of altered bipolar cell populations from rod and ON to OFF-like bipolar cell phenotypes in both the human and the TgP347L rabbit supports previous findings (Marc et al., 2007) and indicates a common theme or mechanism responsible for maintaining bipolar cell viability in the face of loss of afferent input. The presence of cones appears to prevent the onset of gross retinal remodeling and preserves iGluR-coupled signaling to horizontal and bipolar cells, perhaps slowing retinal degenerations. The cone-sparing RPs are slower retinal degenerations, and the overall laminar topology of the retina appears to be maintained in regions underlying surviving cones, even when those cones no longer express opsins (Marc et al., 2007).

DISCUSSION

Retinal remodeling is a phenomenon that occurs subsequent to deafferentation of the neural retina (Jones et al., 2003) and occurs in three phases (Jones et al., 2003; Marc and Jones, 2003). Phase 1 in cone-sparing diseases like those represented in the TgP347L rabbit consists of alteration of bipolar cell iGluR expression that alters their pharmacology, functionally shifting them from ON to OFF phenotypes (Marc et al., 2007). Rhodopsin delocalization in rod photoreceptors also occurs during this phase (Milam et al., 1998) as well as in cones. Phase 2 is heralded by photoreceptor death and Müller cell hypertrophy along with the collapse of the distal Müller cell structure invested in and around the former

Figure 10. Excitation mapping. Each panel is a triplet of γGE :: rgb mapping (left), τBE :: rgb mapping where B (green) is the AGB excitation signal generated by 25 μm KA (middle), and a theme map of cell classes (right). Key: light blue, ganglion cells; bright red, GABAergic amacrine cells; bright green, glycinergic amacrine cells; dark red, OFF bipolar cells; olive green, ON cone bipolar cells; dark blue, rod bipolar cells; tan, horizontal cells. A: Wild-type rabbit. B: A 12-week TgP347L rabbit. C: A 40-week TgP347L rabbit. D,E: Horizontal sections through the bipolar cell layer of (D) wild-type and (E) 40-week TgP347L rabbit retinas visualized with GBE :: rgb mapping demonstrating that 56% of the remaining bipolar cells are AGB responsive. F: Scaled univariate butterfly histograms of KA-activated bipolar cell signals for wild-type type rabbit and 40-week old TgP347L rabbit retinas. Left wing (wild-type rabbit): OFF bipolar cells (pale blue) comprise 37% and nonresponsive ON cone and rod bipolar cells (pale blue and red striped) comprise 63% of all bipolar cells in normal peripheral primate retina. Right wing (40-week TgP347L rabbit): OFF bipolar cells (pale blue) comprise 56% and nonresponsive ON cone bipolar cells (tan) comprise 43% of all remaining bipolar cells in the dystrophic retina. Rod bipolar cells (red) comprise 1% of the remnant cells. For abbreviations, see list. Scale bar = 20 μm in A–E.

C
O
L
O
R
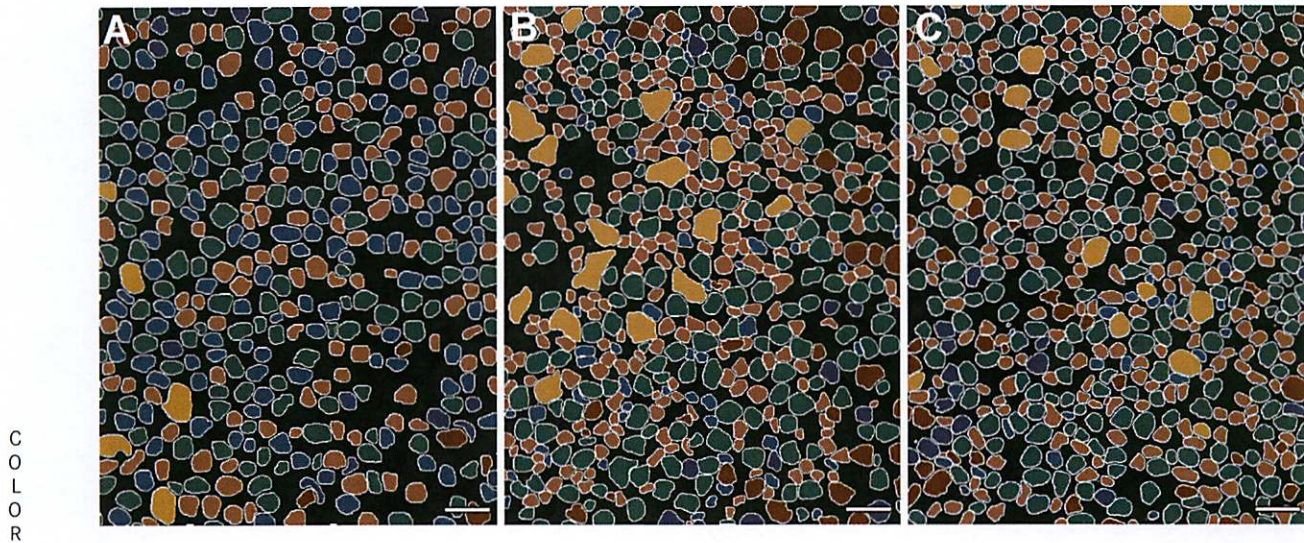
Figure 11. Theme maps of horizontal sections through ONL. **A–C:** KA-driven (25 μm) signaling in (A) wild-type, (B) 12-week TgP347L rabbit, and (C) 40-week TgP347L rabbit retinas clustered and segmented through computational molecular phenotyping (CMP). Cell classes include rod bipolar cells (light blue), ON cone bipolar cells (light red), OFF cone bipolar cells (green), glycinergic amacrine cells (dark blue), GABAergic amacrine cells (dark red), and horizontal cells (orange). Müller cells are black. Scale bar = 30 μm in A–C.

photoreceptor cell bodies (Jones et al., 2003, 2005; Marc and Jones, 2003; Jones and Marc, 2005). Bipolar cells are completely deafferented in phase 2 through molecular changes in iGluR expression (Marc et al., 2007) as well as structural changes to dendritic fields. Additionally, phase 2 brings anomalous sprouting of processes from bipolar and horizontal cells (Strettoi and Pignatelli, 2000; Strettoi et al., 2002, 2003). Phase 3 brings fundamental topologic reorganization of the neural retina, forever altering the lamination of the retina through bidirectional migration of neurons throughout the vertical axis of the neural retina. Microneuroma formation also occurs in phase 3 as retinal neurons elaborate processes that co-fasciculate and elaborate tufts of novel neuropil (Jones et al., 2003, 2005, 2006; Marc and Jones, 2003; Marc et al., 2003, 2005a; Jones and Marc, 2005). Late in phase 3, the borders of the neural retina break down, allowing neural emigration out of the retina into the choroid (Marc et al., 2008).

The TgP347L rabbit model of adRP (Kondo et al., 2009) is the first transgenic rabbit model of retinal degeneration and represents a new tool in the exploration of adRP mechanisms and therapeutic interventions. Further, the TgP347L rabbit exhibits disease progression closely mimicking forms of human RP (Jones et al., 2003; Marc and Jones, 2003; Marc et al., 2003, 2007; Marc, 2010).

Basic degeneration

The model shows, similar to human RP (Marc et al., 2007), progressive and mosaiced rod-specific degenera-

tion, with some regions maintaining relative rod survival, others showing cone sparing, and yet other regions losing all photoreceptors. The mosaic pattern may be due to regional variation in transgene opsin expression, but even human RP retinas show patterned degeneration. ERG demonstrates progressive, rod-dominant degeneration (Kondo et al., 2009) with larger oscillatory potentials in the TgP347L rabbit suggesting alterations in inner retinal neurons (Sakai et al., 2009) consistent with the idea that the remodeling and reprogramming may begin long before structural changes are evident.

Automated TEM imaging (Anderson et al., 2009) shows vesicular debris and outer segment fragments suggestive of trafficking defects. Regardless of the mechanism for debris accumulation in the subretinal space, it appears to be ineffectively cleared by the RPE (Fig. 3E,F), and presumed macrophages appear in retinal degenerations (Fig. 6, box). Small, weakly rhodopsin-immunoreactive vesicles in the subretinal 12–16-week-old rabbit retina (Fig. 3B,E,F) do not appear to arise directly from photoreceptor outer segments (Kondo et al., 2009), although they are similar to those seen in TgP347S transgenic mice (Li et al., 1996). Other mechanisms of photoreceptor cell death may be involved, including rhodopsin overproduction (Olsson et al., 1992; Tan et al., 2001), prolonged phototransduction events (Chen et al., 1995), or mislocalized opsin (Alfinito and Townes-Anderson, 2002).

If buildup of rhodopsin is itself cytotoxic in the subretinal space, this suggests some tantalizing clinical therapeutic interventions including surgical retinal detachment

followed by lavage to clear cytotoxic debris. Although speculative, this experiment is ideally performed in the TgP347L rabbit as opposed to rat or mouse models, as the large eye of the rabbit is the preferred model to test this and other potential therapeutic interventions prior to clinical trials, including potential late-stage gene knockdowns on patients to reduce rhodopsin expression This of course presumes that the vesicular rhodopsin "froth" in the subretinal space of the TgP347L rabbit is not a result of rhodopsin overexpression (4:1 in the line 7 TgP347L rabbit) and will depend on a similar finding of rhodopsin debris in human patients, which so far has not been described in the literature. However, images in previously published papers (Bonilha et al., 2005) appear to indicate the presence of rhodopsin froth with light microscopic analysis. Ultrastructural analysis of early to mid-stage human RP tissues would be required to confirm this.

Metabolic changes

Similar to retinal detachment (Marc et al., 1998a), Müller cells in the TgP347L rabbit show altered metabolic profiles (Figs. 8–10) and gross regional variation in GS and CRALBP expression (Fig. 9C,F), possibly recapitulating developmental programming (Moscona and Kirk, 1965). Individual Müller cells may be responding to microenvironmental osmotic/oxidative challenges, or they may have lost previously unknown coordination signals. Signatures are changing in 16-week TgP347L rabbit Müller cells (Fig. 7) long before they become hypertrophic or engage in seal formation, representing early stress markers. GS expression in the TgP347L rabbit (Fig. 9C) is significantly upregulated in a mosaiced fashion in degenerate retina in marked contrast to results reported in RCS rat retina (Hartig et al., 1995) and in light-damaged retina (Grosche et al., 1997). Paradoxically, this is in contrast to proposed mechanisms (Germer et al., 1997) that might predict decreases in GS after photoreceptor loss due to GS being substrate regulated. However, it could be reasoned that retinal glutamate-dominated superclasses at this stage of degeneration could be releasing glutamate, and that Müller cells sampling the environment around former and novel synaptic contacts are responding to local microdomains. Coherency and aggressiveness of the degeneration may be responsible for Müller cell reactivity and because the TgP347L rabbit still possesses cone photoreceptors in many locations at 40 weeks, reactive gliosis and subsequent changes observed in metabolic signals may be more prolonged than in the coherent RCS rat model (Jones et al., 2003).

Remodeling

Rod degeneration is complete in regions by 40 weeks. The presence of deconstructed survivor cones prevents onset of phase 3 remodeling and preserves iGluR-coupled signaling to horizontal and bipolar cells. Not all remodeling is prevented, as horizontal cells demonstrate extensive anomalous axonogenesis, identical to rodent retinal degenerations (Strettoi et al., 2003) and cat models of retinal detachment (Lewis et al., 1998; Marc et al., 1998a). Whether this poses functional consequences for retinal processing is uncertain, but it suggests that stress signals for remodeling are present and may affect other cell classes.

There are two horizontal cell classes in the rabbit retina (Dacheux and Raviola, 1982). We presume that remodeling horizontal cells are type A due to strong calbindin labeling (Johnson and Vardi, 1998), but cannot reject the possibility that calbindin expression in type B horizontal cells is upregulated in degenerate retina (Fig. 9B,E). Type B horizontal cells also express calbindin, albeit at low levels (Massey and Mills, 1996). Horizontal cell body hypertrophy and sprouting in the postdevelopmental state in response to deafferentation from rod photoreceptors is observed, similar to the rd1 mouse (Strettoi et al., 2002). Horizontal cell axonal morphology is regulated by rod photoreceptors (Raven et al., 2007) during development, but it could be reasoned that if afferent input were removed in the degenerative state, horizontal cells would continue to monitor their environment and respond by sprouting. Indeed, in these preparations, horizontal cells deviate extensively from expected lamination, extending into the IPL, demonstrating continued plasticity well into adulthood (Fig. 9B,E).

The TgP347L rabbit at 40 weeks is on the cusp of phase 3 remodeling with active neuritogenesis in bipolar, amacrine, and horizontal cells (Figs. 8, 10, 11). Gross neuronal migration throughout the retina (Jones et al., 2003; Marc et al., 2003) and reprogramming of bipolar cells is nearly complete (Figs. 12, 13), and microneuromas are evident (Figs. 4E,F, 8E,G, 10C–F, 11B,D,E, 12B,C). PKC labeling demonstrates alterations in normal projections of bipolar cells (Fig. 9D), with axons projecting along the border of the IPL rather than appropriately terminating in the amacrine cell layer (ACL) or ganglion cell layer (GCL). Some of these may be extranumerary axons forming in response to dendritic and morphological revision (Marc et al., 2007).

AQ5

In late retinal degeneration, loss of the outer nuclear layer initiates gross topographic retinal remodeling with changes in cell populations and connectivity. These changes occur with elaboration of a Müller cell seal followed by inversions of bipolar cells and amacrine cells to the GCL, migrations of amacrine cells to the distal retina by the subretinal space, and occasionally ganglion cell migration into the amacrine cell layer (ACL). In the TgP347L rabbit at 40 weeks, these changes associated

with retinal remodeling are beginning, with the elaboration of the Müller cell seal (Figs. 5D, 8H, 10A,B, 11F, 12C).

A number of studies indicate alterations in bipolar and horizontal cell sprouting including retinal detachment from the RPE (Lewis et al., 1998), human RP (Li et al., 1995) and the RCS rat model (Cuenca et al., 2005) along with functional reprogramming of retinal cell populations in human (Marc et al., 2007). In all of these separate models of retinal degeneration, negative plasticity ensues following a common theme, deafferentation.

Reprogramming

Of clinical import to preservation of vision and restorative therapeutics, all forms of cone-sparing RP (rodent, rabbit, porcine, human) demonstrate reprogramming of survivor bipolar cells. Some evidence for reprogramming is anatomic, in the form of new bipolar cell dendrites, some of which make ectopic contacts with cones (Peng et al., 2000; Cuenca et al., 2004). Functional evidence of reprogramming is identical in rodents, humans (Marc et al., 2007), and, now, rabbits. In human and rabbit retina in particular, the fraction of KA-responsive cones increases by a factor of 2–3. Because expression of functional KA or AMPA receptors for sign-conserving cone → bipolar cell signaling is the sin qua non for OFF pathways, display of KA-activated AGB permeation is a robust test of retinal OFF bipolar cells (Marc, 1999c). The increase in the fraction of OFF bipolar cells is so large that it can only be explained as a formal phenotype switch by ON bipolar cells. In human retina, all rod bipolar cells switch from ON to OFF pharmacologies (Marc et al., 2007). In the TgP347L rabbit, the switch is even more extreme, and the fraction of OFF-responsive cells can only be accounted for if some ON cone bipolar cells also switch phenotypes. This difference may be due to the fact that the extent of cone loss in the rabbit is far more severe than in our samples of human RP. Why this would trigger a phenotype switch is uncertain. We previously hypothesized that one trigger for the switch to higher affinity receptors (iGluR vs. mGluR6) may be due to lowered synaptic glutamate availability (Marc et al., 2007).

In summary, although there are some differences between the lagomorph and primate retinas including the lack of a retinal vasculature in the lagomorph and a lack of a true fovea, the TgP347L transgenic rabbit model of RP has become the ideal model for human adRP, providing all the advantages of a large-eye model in developing therapeutic interventions of inherited blinding diseases, which is critical to translational medicine. This model demonstrates disease progression mimicking human disease, including alterations of circuitry and subsequent triggering of retinal remodeling and neural reprogramming. The TgP347L rabbit exhibits relatively fast disease progression, with photoreceptors degenerating by 40 weeks, making the TgP347L rabbit a superior model for cell biological, progenitor cell transplantation, and surgical and bionic prosthetic studies.

LITERATURE CITED

Acland GM, Aguirre GD, Ray J, Zhang Q, Aleman TS, Cideciyan AV, Pearce-Kelling SE, Anand V, Zeng Y, Maguire AM, Jacobson SG, Hauswirth WW, Bennett J. 2001. Gene therapy restores vision in a canine model of childhood blindness. Nat Genet 28:92–95.

Alfinito PD, Townes-Anderson E. 2002. Activation of mislocalized opsin kills rod cells: a novel mechanism for rod cell death in retinal disease. Proc Natl Acad Sci U S A 99: 5655–5660.

Anderson DH, Neitz J, Saari JC, Kaska DD, Fenwick J, Jacobs GH, Fisher SK. 1986. Retinoid-binding proteins in cone-dominant retinas. Invest Ophthalmol Vis Sci 27:1015–1026.

Anderson JR, Jones BW, Yang J-H, Shaw MV, Watt CB, Koshevoy P, Spaltenstein J, Jurrus E, Uv K, Whitaker RT, Mastronarde D, Tasdizen T, Marc RE. 2009. A computational framework for ultrastructural mapping of neural circuitry. PLoS Biol 7:e1000074.

Baehr W, Frederick JM. 2009. Naturally occurring animal models with outer retina phenotypes. Vision Res 49:2636–2652.

Bainbridge JW, Smith AJ, Barker SS, Robbie S, Henderson R, Balaggan K, Viswanathan A, Holder GE, Stockman A, Tyler N, Petersen-Jones S, Bhattacharya SS, Thrasher AJ, Fitzke FW, Carter BJ, Rubin GS, Moore AT, Ali RR. 2008. Effect of gene therapy on visual function in Leber's congenital amaurosis. N Engl J Med 358:2231–2239.

Banin E, Cideciyan AV, Aleman TS, Petters RM, Wong F, Milam AH, Jacobson SG. 1999. Retinal rod photoreceptor-specific gene mutation perturbs cone pathway development. Neuron 23:549–557.

Beltran WA, Wen R, Acland GM, Aguirre GD. 2007. Intravitreal injection of ciliary neurotrophic factor (CNTF) causes peripheral remodeling and does not prevent photoreceptor loss in canine RPGR mutant retina. Exp Eye Res 84: 753–771.

Bonilha VL, Hollyfield JG, Grover S, Fishman GA. 2005. Abnormal distribution of red/green cone opsins in a patient with an autosomal dominant cone dystrophy. Ophthalmic Genet 26:69–76.

Bunt-Milam AH, Saari JC. 1983. Immunocytochemical localization of two retinoid-binding proteins in vertebrate retina. J Cell Biol 97:703–712.

Celio MR, Baier W, Scharer L, Gregersen HJ, de Viragh PA, Norman AW. 1990. Monoclonal antibodies directed against the calcium binding protein calbindin D-28k. Cell Calcium 11:599–602.

Chader GJ. 2002. Animal models in research on retinal degenerations: past progress and future hope. Vision Res 42: 393–399.

Chen J, Makino CL, Peachey NS, Baylor DA, Simon MI. 1995. Mechanisms of rhodopsin inactivation in vivo as revealed by a COOH-terminal truncation mutant. Science 267:374–377.

Crooks J, Kolb H. 1992. Localization of GABA, glycine, glutamate and tyrosine hydroxylase in the human retina. J Comp Neurol 315:287–302.

Cuenca N, Pinilla I, Sauvé Y, Lu B, Wang S, Lund RD. 2004. Regressive and reactive changes in the connectivity

patterns of rod and cone pathways of P23H transgenic rat retina. Neuroscience 127:301–317.

Dacheux RF, Raviola E. 1982. Horizontal cells in the retina of the rabbit. J Neurosci 2:1486–1493

Davanger S, Ottersen OP, Storm-Mathisen J. 1991. Glutamate, GABA, and glycine in the human retina: an immunocytochemical investigation. J Comp Neurol 311:483–494.

Eckhorn R, Wilms M, Schanze T, Eger M, Hesse L, Eysel UT, Kisvarday ZF, Zrenner E, Gekeler F, Schwahn H, Shinoda K, Sachs H, Walter P. 2006. Visual resolution with retinal implants estimated from recordings in cat visual cortex. Vision Res 46:2675–2690.

Faktorovich EG, Steinberg RH, Yasumura D, Matthes MT, LaVail MM. 1990. Photoreceptor degeneration in inherited retinal dystrophy delayed by basic fibroblast growth factor. Nature 347:83–86.

Faktorovich EG, Steinberg RH, Yasumura D, Matthes MT, LaVail MM. 1992. Basic fibroblast growth factor and local injury protect photoreceptors from light damage in the rat. J Neurosci 12:3554–3567.

Fariss RN, Li ZY, Milam AH. 2000. Abnormalities in rod photoreceptors, amacrine cells, and horizontal cells in human retinas with retinitis pigmentosa. Am J Ophthalmol 129:215–223.

Fischer AJ, Stanke JJ, Aloisio G, Hoy H, Stell WK. 2007. Heterogeneity of horizontal cells in the chicken retina. J Comp Neurol 500:1154–1171.

Gargini C, Terzibasi E, Mazzoni F, Strettoi E. 2007. Retinal organization in the retinal degeneration 10 (rd10) mutant mouse: a morphological and ERG study. J Comp Neurol 500:222–238.

Germer A, Jahnke C, Mack A, Enzmann V, Reichenbach A. 1997. Modification of glutamine synthetase expression by mammalian Muller (glial) cells in retinal organ cultures. Neuroreport 8:3067–3072.

Gias C, Jones M, Keegan D, Adamson P, Greenwood J, Lund R, Martindale J, Johnston D, Berwick J, Mayhew J, Coffey P. 2007. Preservation of visual cortical function following retinal pigment epithelium transplantation in the RCS rat using optical imaging techniques. Eur J Neurosci 25:1940–1948.

Grosche J, Grimm D, Clemens N, Reichenbach A. 1997. Retinal light damage vs. normal aging of rats: altered morphology, intermediate filament expression, and nuclear organization of Muller (glial) cells. J Hirnforsch 38:459–470.

Grunert U, Martin PR. 1991. Rod bipolar cells in the macaque monkey retina: immunoreactivity and connectivity. J Neurosci 11:2742–2758.

Grunert U, Wassle H. 1990. GABA-like immunoreactivity in the macaque monkey retina: a light and electron microscopic study. J Comp Neurol 297:509–524.

Hartig W, Grosche J, Distler C, Grimm D, el-Hifnawi E, Reichenbach A. 1995. Alterations of Muller (glial) cells in dystrophic retinae of RCS rats. J Neurocytol 24:507–517.

Haverkamp S, Wässle H. 2000. Immunocytochemical analysis of the mouse retina. J Comp Neurol 424:1–23.

Haverkamp S, Wässle H, Duebel J, Kuner T, Augustine GJ, Feng G, Euler T. 2005. The primordial, blue-cone color system of the mouse retina. J Neurosci 25:5438–5445.

Hendrickson A, Troilo D, Djajadi H, Possin D, Springer A. 2009. Expression of synaptic and phototransduction markers during photoreceptor development in the marmoset monkey *Callithrix jacchus*. J Comp Neurol 512:218–231.

Hicks D, Molday RS. 1986. Differential immunogold-dextran labeling of bovine and frog rod and cone cells using monoclonal antibodies against bovine rhodopsin. Exp Eye Res 42:55–71.

Humayun MS, de Juan E Jr, Dagnelie G, Greenberg RJ, Propst RH, Phillips DH. 1996. Visual perception elicited by electrical stimulation of retina in blind humans. Arch Ophthalmol 114:40–46.

Johnson MA, Vardi N. 1998. Regional differences in GABA and GAD immunoreactivity in rabbit horizontal cells. Vis Neurosci 15:743–753.

Jones BW, Marc RE. 2005. Retinal remodeling during retinal degeneration. Exp Eye Res 81:123–137.

Jones BW, Watt CB, Frederick JM, Baehr W, Chen CK, Levine EM, Milam AH, LaVail MM, Marc RE. 2003. Retinal remodeling triggered by photoreceptor degenerations. J Comp Neurol 464:1–16.

Jones BW, Watt CB, Marc RE. 2005. Retinal remodelling. Clin Exp Optom 88:282–291.

Jones BW, Marc RE, Watt CB, Vaughan DK, Organisciak DT. 2006. Neural plasticity revealed by light-induced photoreceptor lesions. Adv Exp Med Biol 572:405–410.

Kalloniatis M, Fletcher EL. 1993. Immunocytochemical localization of the amino acid neurotransmitters in the chicken retina. J Comp Neurol 336:174–193.

Kalloniatis M, Marc RE, Murry RF. 1996. Amino acid signatures in the primate retina. J Neurosci 16:6807–6829.

Kalloniatis M, Sun D, Foster L, Haverkamp S, Wässle H. 2004. Localization of NMDA receptor subunits and mapping NMDA drive within the mammalian retina. Vis Neurosci 21:587–597.

Karschin A, Wässle H. 1990. Voltage- and transmitter-gated currents in isolated rod bipolar cells of rat retina. J Neurophysiol 63:860–876.

Kondo M, Sakai T, Komeima K, Kurimoto Y, Ueno S, Nishizawa Y, Usukura J, Fujikado T, Tano Y, Terasaki H. 2009. Generation of a transgenic rabbit model of retinal degeneration. Invest Ophthalmol Vis Sci 50:1371–1377.

Lakhanpal RR, Yanai D, Weiland JD, Fujii GY, Caffey S, Greenberg RJ, de Juan E Jr, Humayun MS. 2003. Advances in the development of visual prostheses. Curr Opin Ophthalmol 14:122–127.

Lewis GP, Linberg KA, Fisher SK. 1998. Neurite outgrowth from bipolar and horizontal cells after experimental retinal detachment. Invest Ophthalmol Vis Sci 39:424–434.

Li T, Snyder WK, Olsson JE, Dryja TP. 1996. Transgenic mice carrying the dominant rhodopsin mutation P347S: evidence for defective vectorial transport of rhodopsin to the outer segments. Proc Natl Acad Sci U S A 93:14176–14181.

Li W, Keung JW, Massey SC. 2004. Direct synaptic connections between rods and OFF cone bipolar cells in the rabbit retina. J Comp Neurol 474:1–12.

Li ZY, Kljavin IJ, Milam AH. 1995. Rod photoreceptor neurite sprouting in retinitis pigmentosa. J Neurosci 15:5429–5438.

Maguire AM, Simonelli F, Pierce EA, Pugh EN Jr, Mingozzi F, Bennicelli J, Banfi S, Marshall KA, Testa F, Surace EM, Rossi S, Lyubarsky A, Arruda VR, Konkle B, Stone E, Sun J, Jacobs J, Dell'Osso L, Hertle R, Ma JX, Redmond TM, Zhu X, Hauck B, Zelenaia O, Shindler KS, Maguire MG, Wright JF, Volpe NJ, McDonnell JW, Auricchio A, High KA, Bennett J. 2008. Safety and efficacy of gene transfer for Leber's congenital amaurosis. N Engl J Med 358:2240–2248.

Marc RE. 1999a. Kainate activation of horizontal, bipolar, amacrine, and ganglion cells in the rabbit retina. J Comp Neurol 407:65–76.

Marc RE. 1999b. Mapping glutamatergic drive in the vertebrate retina with a channel-permeant organic cation. J Comp Neurol 407:47–64.

Marc RE. 1999c. Subtypes of Off center bipolar cells possess different ionotropic glutamate receptor channel properties. Invest Ophthalmol Vis Sci 40:4159.

Marc RE. 2010. Injury and repair: retinal remodeling. In: Dartt DA, editor. Encyclopedia of the eye. New York: Elsevier. p 414–420.

Marc RE, Cameron DA. 2002. A molecular phenotype atlas of the zebrafish retina. J Neurocytol 321:649–666.

Marc RE, Jones BW. 2002. Molecular phenotyping of retinal ganglion cells. J Neurosci 22:413–427.

Marc RE, Jones BW. 2003. Retinal remodeling in inherited photoreceptor degenerations. Mol Neurobiol 28:139–147.

Marc RE, Murry RF, Basinger SF. 1995. Pattern recognition of amino acid signatures in retinal neurons. J Neurosci 15: 5106–5129.

Marc RE, Murry RF, Fisher SK, Linberg KA, Lewis GP. 1998a. Amino acid signatures in the detached cat retina. Invest Ophthalmol Vis Sci 39:1694–1702.

Marc RE, Murry RF, Fisher SK, Linberg KA, Lewis GP, Kalloniatis M. 1998b. Amino acid signatures in the normal cat retina. Invest Ophthalmol Vis Sci 39:1685–1693.

Marc RE, Jones BW, Watt CB, Strettoi E. 2003. Neural remodeling in retinal degeneration. Prog Retina Eye Res 22:607–655.

Marc RE, Jones BW, Watt CB. 2005a. Retinal remodeling: circuitry revisions triggered by photoreceptor degeneration. New York: Springer/Kluwer Academic Press.

Marc RE, Kalloniatis M, Jones BW. 2005b. Excitation mapping with the organic cation AGB2+. Vision Res 45:3454–3468.

Marc RE, Jones BW, Anderson JR, Kinard K, Marshak DW, Wilson JH, Wensel T, Lucas RJ. 2007. Neural reprogramming in retinal degeneration. Invest Ophthalmol Vis Sci 48:3364–3371.

Marc RE, Jones BW, Watt CB, Vazquez-Chona F, Vaughan DK, Organisciak DT. 2008. Extreme retinal remodeling triggered by light damage: implications for age related macular degeneration. Mol Vision 14:782–806.

Martin PR, Grunert U. 1992. Spatial density and immunoreactivity of bipolar cells in the macaque monkey retina. J Comp Neurol 323:269–287.

Massey SC, Mills SL. 1996. A calbindin-immunoreactive cone bipolar cell type in the rabbit retina. J Comp Neurol 366: 15–33.

Milam AH, Li ZY, Fariss RN. 1998. Histopathology of the human retina in retinitis pigmentosa. Prog Retin Eye Res 17:175–205.

Molday RS, MacKenzie D. 1983. Monoclonal antibodies to rhodopsin: characterization, cross-reactivity, and application as structural probes. Biochemistry 22:653–660.

Moscona AA, Kirk DL. 1965. Control of glutamine synthetase in the embryonic retina in vitro. Science 148:519–521.

Olsson JE, Gordon JW, Pawlyk BS, Roof D, Hayes A, Molday RS, Mukai S, Cowley GS, Berson EL, Dryja TP. 1992. Transgenic mice with a rhodopsin mutation (Pro23His): a mouse model of autosomal dominant retinitis pigmentosa. Neuron 9:815–830.

Otani A, Dorrell MI, Kinder K, Moreno SK, Nusinowitz S, Banin E, Heckenlively J, Friedlander M. 2004. Rescue of retinal degeneration by intravitreally injected adult bone marrow-derived lineage-negative hematopoietic stem cells. J Clin Invest 114:765–774.

Peng YW, Hao Y, Petters RM, Wong F. 2000. Ectopic synaptogenesis in the mammalian retina caused by rod photoreceptor-specific mutations. Nat Neurosci 3:1121–1127.

Petersen-Jones SM. 1998. Animal models of human retinal dystrophies. Eye 12:566–570.

Petters RM, Alexander CA, Wells KD, Collins EB, Sommer JR, Blanton MR, Rojas G, Hao Y, Flowers WL, Banin E, Cideciyan AV, Jacobson SG, Wong F. 1997. Genetically engineered large animal model for studying cone photoreceptor survival and degeneration in retinitis pigmentosa. Nat Biotechnol 15:965–970.

Pow DV, Crook DK. 1995. Immunocytochemical evidence for the presence of high levels of reduced glutathione in radial glial cells and horizontal cells in the rabbit retina. Neurosci Lett 193:25–28.

Raven MA, Oh EC, Swaroop A, Reese BE. 2007. Afferent control of horizontal cell morphology revealed by genetic respecification of rods and cones. J Neurosci 27:3540–3547.

Sakai T, Kondo M, Ueno S, Koyasu T, Komeima K, Terasaki H. 2009. Supernormal ERG oscillatory potentials in transgenic rabbit with rhodopsin P347L mutation and retinal degeneration. Invest Ophthalmol Vis Sci 50:4402–4409.

Sarthy V, Bickoff C. 1996. Immunocytochemical localization of retinoid-binding protein in the dogfish retina. Curr Eye Res 15:905–907.

Sasaki T, Kaneko A. 1996. L-Glutamate-induced responses in OFF-type bipolar cells of the cat retina. Vision Res 36: 787–795.

Slaughter MM, Miller RF. 1981. 2-Amino-4-phosphonobutyric acid: a new pharmacological tool for retina research. Science 211:182–185.

Slaughter MM, Miller RF. 1983. Bipolar cells in the mudpuppy retina use an excitatory amino acid neurotransmitter. Nature 303:537–538.

Strettoi E, Pignatelli V. 2000. Modifications of retinal neurons in a mouse model of retinitis pigmentosa. Proc Natl Acad Sci U S A 97:11020–11025.

Strettoi E, Porciatti V, Falsini B, Pignatelli V, Rossi C. 2002. Morphological and functional abnormalities in the inner retina of the rd/rd mouse. J Neurosci 22:5492–5504.

Strettoi E, Pignatelli V, Rossi C, Porciatti V, Falsini B. 2003. Remodeling of second-order neurons in the retina of rd/rd mutant mice. Vision Res 43:867–877.

Tan E, Wang Q, Quiambao AB, Xu X, Qtaishat NM, Peachey NS, Lem J, Fliesler SJ, Pepperberg DR, Naash MI, Al-Ubaidi MR. 2001. The relationship between opsin overexpression and photoreceptor degeneration. Invest Ophthalmol Vis Sci 42:589–600.

Vardi N, Duvoisin R, Wu G, Sterling P. 2000. Localization of mGluR6 to dendrites of ON bipolar cells in primate retina. J Comp Neurol 423:402–412.

Vugler A, Lawrence J, Walsh J, Carr A, Gias C, Semo M, Ahmado A, da Cruz L, Andrews P, Coffey P. 2007. Embryonic stem cells and retinal repair. Mech Dev 124:807–829.

Wang Y, Macke JP, Merbs SL, Zack DJ, Klaunberg B, Bennett J, Gearhart J, Nathans J. 1992. A locus control region adjacent to the human red and green visual pigment genes. Neuron 9:429–440.

Wässle H, Boycott BB. 1991. Functional architecture of the mammalian retina. Physiol Rev 71:447–480.

Wulle I, Wagner HJ. 1990. GABA and tyrosine hydroxylase immunocytochemistry reveal different patterns of colocalization in retinal neurons of various vertebrates. J Comp Neurol 296:173–178.

Yamashita M, Wässle H. 1991. Responses of rod bipolar cells isolated from the rat retina to the glutamate agonist 2-amino-4-phosphonobutyric acid (APB). J Neurosci 11:2372–2382.

Yan RT, Liang L, Ma W, Li X, Xie W, Wang SZ. 2010. Neurogenin1 effectively reprograms cultured chick retinal pigment epithelial cells to differentiate toward photoreceptors. J Comp Neurol 518:526–546.

Yanai D, Weiland JD, Mahadevappa M, Greenberg RJ, Fine I, Humayun MS. 2007. Visual performance using a retinal prosthesis in three subjects with retinitis pigmentosa. Am J Ophthalmol 143:820–827.

Young MJ, Ray J, Whiteley SJ, Klassen H, Gage FH. 2000. Neuronal differentiation and morphological integration of hippocampal progenitor cells transplanted to the retina of immature and mature dystrophic rats. Mol Cell Neurosci 16:197–205.

Zeiss CJ, Allore HG, Towle V, Tao W. 2006. CNTF induces dose-dependent alterations in retinal morphology in normal and rcd-1 canine retina. Exp Eye Res 82:395–404.

My edits:

Author "Jia Hui Yang" should be "Jia-Hui Yang"

AQ1:

466-8560

AQ2:

"Edward N. and Della L. Thome Memorial Foundation grant for Age-Related Macular Degeneration Research (to B.W.J.), Research to Prevent Blindness Career Development Award (to B.W.J.), Moran Eye Center Tiger Team Translational Medicine Award (to B.W.J.); Grant sponsor: National Institutes of Health; Grant numbers: EY015128 (to R.M.), EY02576 (to R.M.), and EYO14800; Grant sponsor: Vision Core, an unrestricted grant from Research to Prevent Blindness to the Moran Eye Center; Grant sponsor: National Science Foundation; Grant number: 0941717 (to R.M.); Grant sponsor: the Japanese Ministry of Health, Labor, and Welfare; Grant number: Sciences Research Grant H16-sensory-001 (to M.K.)."

Should be:

"Edward N. and Della L. Thome Memorial Foundation grant for Age-Related Macular Degeneration Research (to B.W.J.), Research to Prevent Blindness Career Development Award (to B.W.J.), Moran Eye Center Tiger Team Translational Medicine Award (to B.W.J.); National Institutes of Health EY015128 (to R.E.M.), EY02576 (to R.E.M.), and EYO14800 Vision Core, an unrestricted grant from Research to Prevent Blindness to the Moran Eye Center; National Science Foundation 0941717 (to R.E.M.); The Japanese Ministry of Health, Labor, and Welfare, Sciences Research Grant H16-sensory-001 (to M.K.)."

AQ3:

GCL should be "Ganglion cell layer"
INL should be "Inner nuclear layer"
KA should be "kainic acid"
ONL should be "Outer nuclear layer"

AQ4:

Yes, Phosphate for potophate. Thanks for that catch.

AQ5:

"The TgP347L rabbit at 40 weeks is on the cusp of phase 3 remodeling with active neuritogenesis in bipolar, amacrine, and horizontal cells (Figs. 8, 10, 11). Gross neuronal migration throughout the retina (Jones et al., 2003; Marc et al., 2003) and reprogramming of bipolar cells is nearly complete (Figs. 12, 13), and microneuromas are evident (Figs. 4E,F, 8E,G, 10C,A-F, 11B,D,E, 12B,C)."

should be:

The TgP347L rabbit at 40 weeks is on the cusp of phase 3 remodeling with active neuritogenesis in bipolar, amacrine, and horizontal cells (Figs. 8, 9, 10). Gross neuronal migration throughout the retina (Jones et al., 2003; Marc et al., 2003) and reprogramming of bipolar cells is nearly complete (Figs. 10, 11), and microneuromas are evident (Figs. 5E,F, 6E,G, 8C,A-F, 9B,D,E, 10B,C).

A06:

Not an acknowledgement. A conflict of interest statement.

A07:

Acceptable changes.

A08: